FERMILAB-PUB-09-654-E

Simple Behavior of Primary Cross Sections for Low Mass Particles in $p\bar{p}$ Collisions at y=0 and $\sqrt{s} = 1.8$ TeV

T. Alexopoulos,[1,*] E.W. Anderson,[2] A.T. Bujak,[3] D.D. Carmony,[3] A.R. Erwin,[1] C. Findeisen,[1] K. Gulbrandsen,[1] L.J. Gutay,[3] A.S. Hirsch,[3] C. Hojvat,[4] J.R. Jennings,[1] C. Loomis,[5] J.M. LoSecco,[6] K.S. Nelson,[1] S.H. Oh,[5] N.T. Porile,[7] R.P. Scharenberg,[3] F. Turkot,[4] W.D. Walker,[5] C.H. Wang,[5] and J. Warchol[6]

[1]*Department of Physics, University of Wisconsin, Madison, WI 53706, USA*
[2]*Department of Physics, Iowa State University, Ames, IA 50011, USA*
[3]*Department of Physics, Purdue University, West Lafayette, IN 47907, USA*
[4]*Fermi National Accelerator Laboratory, Batavia, IL 60510, USA*
[5]*Department of Physics, Duke University, Durham, NC 27706, USA*
[6]*Department of Physics, University of Notre Dame, Notre Dame, IN 46556, USA*
[7]*Department of Chemistry, Purdue University, West Lafayette, IN 47907, USA*

A set of inclusive cross sections at zero rapidity, $d\sigma/dy|_{y=0}$, is presented for $\bar{p}p$ interactions at center of mass energy $\sqrt{s} = 1.8$ TeV. Six elementary particle cross sections are corrected for secondary contributions from decays of higher mass resonances in order to produce a set of primary cross sections. The primary cross sections per spin state are well described by $d\sigma^p/dy|_{y=0} = 0.721 \cdot (\pi \lambda\!\!\!^{-2}_{\pi}) \cdot e^{-m/T}$, where m is the particle rest mass, $T = \hbar c/r_h$, and $r_h = 0.97$ fm. The deuterium production cross section is also described if r_h is replaced by $r_A = r_h A^{1/3}$. The same exponential in m and T describes primary charm fractions in e^+e^- collisions at least up to the J/ψ mass. There is no significant evidence for strangeness or charm suppression if only primary production of light hadrons is considered. There is evidence that the primary cross section for each particle may have the same value for pp and $\bar{p}p$ collisions and that it may have nearly constant values between $\sqrt{s} = 63$ GeV and $\sqrt{s} = 1800$ GeV. Fits to the final state transverse momenta of the particles using a gas model favor a temperature T=132 MeV, a chemical potential $\mu = 129$ MeV, and a transverse flow of the gas with $\beta_f = 0.27$.

PACS numbers: 13.85.Ni,12.40.Ee,13.60.Hb,25.75.Ld,25.75.Nq,25.75.Dw,31.15.Bs,24.10.Ps

I. INTRODUCTION

The experiment E735 at Fermilab studied $p\bar{p}$ collisions in the Tevatron Collider at center of mass energy $\sqrt{s} = 1.8$ TeV. The production of particles and their p_t spectra at rapidity y=0 were recorded along with associated multiplicity and any other accessible information. These results have been published in several articles [1, 2, 3, 4, 5, 6, 7, 8]. A few of the production rates were reported as absolute inclusive cross sections, while others were reported as rates relative to some simultaneously observed production processes. The purpose of this article is to assemble the various rate data and to present them all as absolute cross sections. Such a presentation reveals patterns which are relevant to specific production models such as the statistical model, string model, parton collision models, or the quark gluon plasma.

II. DATA ANALYSIS

During the data taking period the accelerator operators made periodic measurements of accelerator parameters with flying wires [9] and wallcurrent monitors [10] to enable a calculation of our luminosity as a function of time. A careful analysis of the luminosity data was subsequently tabulated by Gelfand, Grosso-Pilcher, and White [11, 12] and made available to experimentalists.

The luminosity data can be used to obtain an absolute cross section for the production of any one particle species from the relation

$$N = \sigma \int_0^T \mathcal{L}(t)\, dt, \tag{1}$$

where $\mathcal{L}(t)$ is the measured luminosity as a function of time, σ is some cross section of interest, and N is the number of events which are associated with that cross section during the time interval T. We have previously used the luminosity tabulations together with Eq.(1) to calculate and publish invariant production cross sections for photons [5], phi mesons [6], deuterium, and tritium [7]. Luminosity issues are discussed in more detail later in this article.

We have repeated our previous analysis of π, K, and p inclusive production with some refinements that were intended to reduce background, minimize tracking losses, and improve resolution in the time-of-flight mass spectra [13]. The new π/p ratio remained within 1.3% of that reported in previous publications, but the relative charged kaon flux increased ∼1.4 standard deviations with the new analysis. Raw data were corrected for detector and trigger efficiencies, trigger pre-scaling, trigger

*Current address: Department of Physics, National Technical University of Athens, Athens, Greece

dead time, and particle loss in 0.09 absorption lengths of the spectrometer arm before the last time-of-flight wall at 4 meters. Absolute cross sections $d\sigma/dy|_{y=0}$ were calculated for these three positively charged particles.

III. MEASURED CROSS SECTIONS

Table I gives a list of measured single particle cross sections as collected from various sources. Column 1 lists the particles studied. Antiparticle cross sections were the same as particle cross sections within errors. However, the cross section for antitritium was not measurable. Errors listed here are the result of convolution of statistical and systematic errors. Information on the associated particle multiplicity and the invariant p_t spectra $d\sigma/dy\,dp_t^2$ for all these particles can be found in references cited in the table.

The cross section listed for inclusive single photon production is twice the inclusive cross section of a charged pion within errors. If one assumes production of a neutral pion is equal to production of a charged pion, this value is consistent with the assertion in reference [5] that single photon production originates with the two-photon decay of the neutral pion and possibly some small admixture of eta decay.

In calculating invariant cross sections for the Λ^0 and Ξ^-, we make use of particle ratios in reference [8] such as $[(\Lambda^0 + \bar{\Lambda}^0)/(p + \bar{p})]$ "in the spectrometer arm". Although it is not explicitly stated in reference [8], these actually are *rapidity* based ratios [14] such as $[dN(\Lambda^0 + \bar{\Lambda}^0)/dy|_{y=0}]/[dN(p + \bar{p})/dy|_{y=0}]$, where dN/dy is the number of particles per unit rapidity.

TABLE I: E735 values of $d\sigma/dy$ at rapidity $y = 0$ for various particles produced in $p\bar{p}$ collisions at $\sqrt{s} = 1.8$ TeV.

Particle	$d\sigma/dy\|_{y=0}$	Reference
γ	114.0 ± 7.8 mb	[5]
π^+	56.0 ± 6.3 mb	this paper
K^+	7.37 ± 0.79 mb	this paper
p	4.37 ± 0.62 mb	this paper
ϕ	0.763 ± 0.202 mb	[6]
Λ^0	1.77 ± 0.41 mb	[8]
Ξ^-	0.282 ± 0.082 mb	[8]
d^+	2.02 ± 0.49 μb	[7]
t^+	0.83 ± 0.34 μb	[7]

In the literature one frequently encounters experimental particle production ratios that appear to be defined by the angular aperture of a detector element. For such cases the ratios quoted are more likely to be formed with $dN/d\eta$ rather than with dN/dy, where $d\eta$ is an interval of pseudorapidity which depends only on production angle and not particle mass. Other discussions of particle production ratios make use of the scaling variable $x = 2p_\ell/\sqrt{s}$ to compute dN/dx, where p_ℓ is the longitudinal component of momentum in the center of mass system.

In order to compare our data with such measurements one can use the approximate conversion factors in Table II to convert our values of dN/dy to $dN/d\eta$ or to dN/dx. In this table we present conversion factors c_η and c_x that can be used to multiply our values of dN/dy for an approximate conversion to η or x variables at y=0.

$$(dN/dy)_{y=0} = (1/c_\eta)(dN/d\eta)_{\eta=0} = (1/c_x)(dN/dx)_{x=0} \quad (2)$$

where
$c_\eta = p_t/\sqrt{p_t^2 + m^2}$ and $c_x = (\sqrt{s}/2)/\sqrt{p_t^2 + m^2}$.

The values of c_η and c_x are approximate to the extent that we have assumed $p_\ell = 0$ and used observed average values of p_t for each particle mass to estimate in Table II the conversion of dy to equivalent $d\eta$ and dx intervals in our experiment.

TABLE II: Columns three and four list factors by which one can multiply dN/dy in this experiment to obtain approximate values of $dN/d\eta$ and dN/dx for the particle masses listed in column one. The average values of particle p_t listed in column two were used to evaluate c_η and c_x.

mass (GeV/c^2)	$<p_t>$ (GeV/c)	c_η	c_x
$\gamma(0)$	0.192 ± 0.007	1.000	4688
$\pi(0.139)$	0.433 ± 0.020	0.952	1978
$K(0.494)$	0.590 ± 0.020	0.768	1170
$p(0.938)$	0.716 ± 0.030	0.607	763
$\phi(1.019)$	0.94 ± 0.26	0.678	649
$\Lambda(1.116)$	0.750 ± 0.025	0.558	670
$\Xi(1.321)$	$0.90^{+0.35}_{-0.22}$	0.563	563

IV. CROSS SECTION CHARACTERIZATION

Figure 1 is a plot of production cross sections versus particle mass from Table I. One observes what appears to be a rough exponential decrease in cross section as the particle mass increases. This decrease is not just some overall energy or phase space limitation. At most about 200 charged particles are observed to be created in a few of the highest multiplicity collisions when the available energy would allow creation of around 6,000 pions, each with a kinetic energy of a pion rest mass. Most of the non diffractive particle production is far from encountering a simple phase space limitation.

Some features of Fig. 1 are noteworthy. The photon cross section is not an independent data point since it is mostly attributable to π^0 production [5]. Likewise electron/positron production is negligible. One can observe electrons in the small momentum window between 50 MeV/c, below which the field of the analysis magnet rejects all charged particles, and 200 MeV/c, above which pions begin having enough energy to reach the final time-of-flight counters. The electron mass peak is sharply defined, but it disappears completely above 250 MeV/c underneath the low mass tail of the pion mass

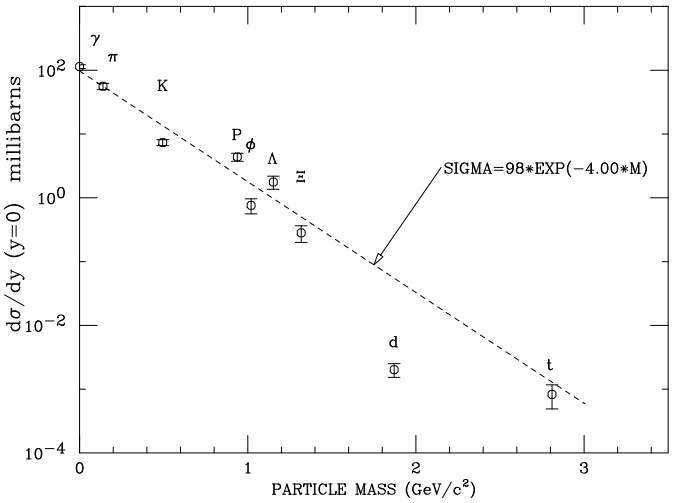

FIG. 1: Cross sections $d\sigma/dy|_{y=0}$ from Table I plotted as a function of particle mass. The dashed line is an arbitrary exponential falloff inserted to guide the eye.

peak. The observed part of the electron flux is consistent with photon conversions in the 2 mm thick aluminum wall of the beam pipe. Since electrons and photons do not participate in the exponentially falling behavior of the cross sections, we will omit them from most of the remaining discussions.

Although the two nuclear cross sections (d and t) are small, as the trend for elementary particles suggests, their behavior may involve unique nuclear effects. We will defer treatment of the nuclear cross sections in a quantitative way for a later section.

V. STRANGENESS SUPPRESSION MODELS

Most strange particle production in Fig. 1 appears systematically suppressed relative to non-strange production even after allowing for some exponential decrease of cross sections with mass. Efforts to characterize this strangeness suppression have a long experimental and theoretical history. A strangeness suppression factor $\lambda = 0.5$ was adopted in the Feynman-Field jet fragmentation model to address this observation in experimental data [15]. Other authors have presented evidence for a value closer to $\lambda = 0.3$ [16, 17].

There is probably nothing fundamental that one can learn from the measured cross sections in Table I without correcting them for secondary contributions that come from higher mass decays. Nevertheless, we have examined the 6 elementary hadron cross sections to see if our data might be made to appear more uniform with respect to mass dependence by using a single strangeness suppression factor λ. To some extent this effort will serve to compare our raw data to that of previous experiments. We have explored 3 variations of strangeness suppression.

We first assumed that if there were no strangeness suppression, all cross sections would be described by

$$\frac{d\sigma}{dy}\Big|_{y=0} = Ae^{-Bm}, \tag{3}$$

where m is the particle rest mass. We then explored variations of strangeness suppression for the following 3 cases: (a) A single divisor λ raises all strange particle cross sections equally. (b) A single divisor λ is applied to measured cross sections for K^+ and Λ^0 because they contain only one strange quark, but a divisor of λ^2 is applied to ϕ and Ξ^- cross sections because each of these particles contains 2 quarks with strangeness quantum numbers. (c) A divisor of λ is applied to K^+, Λ^0, and ϕ cross sections because only one quark pair must be produced to form these particles, but a divisor of λ^2 is applied to the Ξ^- cross section because two quark pairs must be produced to form it.

The data are fitted for values of A, B, and λ that minimize χ^2. The values of χ^2 per degree of freedom for each of the cases listed above are: (a) χ^2_{dof}=4.43, (b) χ^2_{dof}=1.33, (c) χ^2_{dof}=4.37. The best of these fits is case (b), and the dashed line in Fig. 2 shows graphically the extent to which the adjusted strange particle cross sections fit for $\lambda = 0.437$.

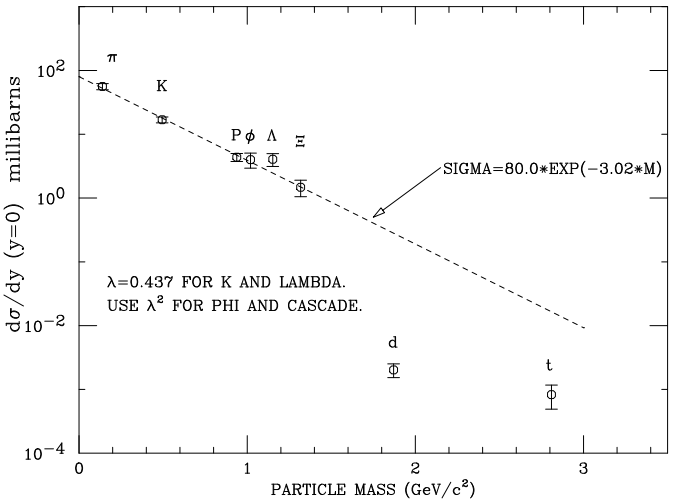

FIG. 2: Six inclusive hadron cross sections of Table I are plotted after multiplying K^+ and Λ^0 cross sections by a factor λ^{-1} and multiplying ϕ and Ξ^- cross sections by a factor λ^{-2}. The best fit to an exponential in mass is the dashed curve for a strangenss suppression value of λ=0.437 with a χ^2_{dof}=1.33.

If we wish to attach some physical significance to the fit such as interpreting the constant B as inverse temperature, then we should use Eq.(4) below instead of Eq.(3)

$$\frac{d\sigma}{dy}\Big|_{y=0} = (2J+1)Ae^{-m/T}, \tag{4}$$

where (2J+1) is the spin degeneracy of a particle or

resonance. To see exponential behavior one must plot $[1/(2J+1)]d\sigma/dy|_{y=0}$. These values of cross section per spin state are given in Table III.

TABLE III: Values of $d\sigma/dy$ at $y = 0$ for hadronic particles produced in this experiment by $p\bar{p}$ collisions at $\sqrt{s} = 1.8$ TeV. Spin degeneracy is removed in the last column.

Particle	Mass (GeV)	$d\sigma/dy\|_{y=0}$	$d\sigma/dy\|_{y=0}/(2J+1)$
π^+	0.139	56.0 ± 6.3 mb	56.0 ± 6.3 mb
K^+	0.494	7.37 ± 0.79 mb	7.37 ± 0.79 mb
p	0.938	4.37 ± 0.62 mb	2.19 ± 0.31 mb
ϕ	1.019	0.763 ± 0.202 mb	0.254 ± 0.067 mb
Λ^0	1.116	1.77 ± 0.41 mb	0.885 ± 0.203 mb
Ξ^-	1.321	0.282 ± 0.082 mb	0.141 ± 0.041 mb
d^+	1.871	2.02 ± 0.49 μb	0.673 ± 0.163 μb
t^+	2.810	0.83 ± 0.34 μb	0.415 ± 0.170 μb

The three cases for a strangeness suppression λ that were discussed above were also fit to the spin-scaled cross sections of Table III. The values of χ^2 per degree of freedom for these three cases were: (a) $\chi^2_{dof} = 10.7$, (b) $\chi^2_{dof} = 3.08$, (c) $\chi^2_{dof} = 12.06$. The best fit is once again for case (b), but the value of χ^2_{dof} is even less satisfactory than the fit to raw data. For this case $\lambda = 0.467$, and interpretation of the mass dependence implies $T = 248 \pm 11$ MeV.

VI. THERMAL DESCRIPTION INCLUDING PARTICLE DECAYS

The assumption of a strangeness suppression factor λ improves the exponential appearance of the data, but it does not return a statistically satisfactory description of the measured data. Also it is not clear if λ results from particle production or particle decay or some combination of the two processes.

It is most certain that particle and resonance *decays* favor pion and proton final states over strange particle final states. Every particle and resonance ultimately results in pions and nucleons, whereas only flavored particles and flavored resonances can decay into strange particles.

We have investigated a thermal model which has no strangeness bias in the production of particles and resonances. It does, however, use the actual strangeness bias found in decays as tabulated by the PDG [18] for 99 of the lowest mass particles and resonances. The model assumes that a particle of given mass is produced in $p\bar{p}$ collisions with equal probability in $(2J+1)$ spin states, $(2I+1)$ isospin states, and particle/antiparticle states. Each spin state for a specified charge is assigned a primary production cross section per spin state according to its rest mass m as in Eq.(5).

$$\frac{d\sigma^p}{dy}\Big|_{y=0} = Ae^{-m/T} \tag{5}$$

Observed particles are considered to result from either primary or secondary production. Primary production cross sections , $d\sigma^p/dy|_{y=0}$, must be estimated using the primary particle mass in Eq.(5) since experimental values for these cross sections are unknown. Secondary contributions are determined by the primary production rates for some higher mass resonances as given in Eq.(5) followed by a variety of branching ratios in their ultimate decay to a primary particle of interest. For low mass particles these branching ratios are very well known and have errors that range from a fraction of a percent to several percent [18].

We are interested in the primary production of a particle because only that rate might be expected to follow the exponential of Eq.(5). Our goal is to learn what fraction x of the measured inclusive cross section for a particle is the result of primary production. Measured cross sections $d\sigma/dy$ can then be related to primary cross sections per spin state $d\sigma^p/dy$ by Eq.(6).

$$(2J+1)\cdot\frac{d\sigma^p}{dy}\Big|_{y=0} = x\cdot\frac{d\sigma}{dy}\Big|_{y=0} \tag{6}$$

The value we find for the fraction x of a particular particle is a function of the assumed temperature T in Eq.(5). For example, when we try to determine the primary π^+ inclusive spectrum, we may find that a massive resonance with large J and I values produces many π^+ mesons by its decay chains, but because its resonance mass is much greater than T, it makes a relatively small secondary contribution to the observed π^+ inclusive spectrum.

Branching ratios, conservation laws, and Clebsch-Gordon coefficients were used to determine how much each primary state contributed to observed π^+, K^+, p, ϕ, Λ^0, and Ξ^- inclusive spectra in the E735 detector. For particles with lifetimes of $\approx 10^{-10}$ seconds it was necessary to use a Monte Carlo program to evaluate average corrections for loss of particles due to detector aperture and analysis cuts. Typically ∼65% of these protons were accepted and ∼15% of these pions. Strong decays give prompt secondary particles at the beamline and were given no relative corrections for the detector losses.

The tableau in Fig. 3 shows, as a function of the mass of a particle/resonance, the relative integrated contributions from various resonances and particles to the 6 inclusive cross sections we are studying. Vertical scales in the figure were chosen arbitrarily in order to illustrate better the limiting contributions from decays of higher masses. The exact shape and limiting values of these curves will have a dependence on the choice of T used in Eq.(5). The value of T was chosen to be 204 MeV in order to produce the set of curves shown. The ratio of the lowest mass step (primary production) to the limiting integrated value yields x, the fraction that is primary production.

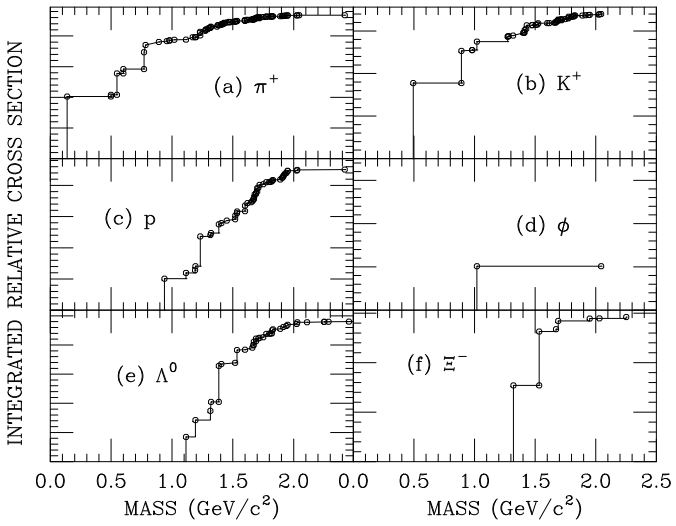

FIG. 3: Six plots are shown for a common assumed value of T. They display relative integrated cross section for a particle as a function of the mass of contributing resonance or particle decays. In general the limiting values of these curves will depend on the choice of T. These plots use the value $T =$ 204 MeV, which minimizes the chi-square fit of primary cross sections per spin state to Eq.(5).

A two parameter fit was done for A and T in Eq.(5) using the 6 inclusive cross sections per spin state in column 4 of Table III. In order to do this it was necessary to make the functional dependence of the primary fraction, x, on T available to the χ^2 fitting program. The fit is excellent with a χ^2 per degree of freedom $\chi^2_{dof} = 0.317$ for 4 degrees of freedom.

Table IV lists for each measured particle the value of x and the primary cross section per spin state as determined by the fit. The primary cross sections per spin state are plotted in Figure 4 along with the fitted function (dashed curve). The temperature determined by the fit is $T = 204 \pm 14$ MeV. This is significantly higher than $T = 160$ MeV suggested for the bootstrap statistical model [19] and quite close to $T = 200$ MeV suggested for the QGP [20].

TABLE IV: Values of $d\sigma/dy$ at $y = 0$ for hadronic particles produced in $p\bar{p}$ collisions at $\sqrt{s} = 1.8$ TeV. Column 2 lists cross sections with spin degeneracy removed. Column 3 lists factors by which column 2 must be multiplied to obtain primary cross sections per spin state listed in column 4.

Particle	$d\sigma/dy\|_{y=0}/(2J+1)$	x	$d\sigma^p/dy\|_{y=0}$(mb)
π^+	56.0 ± 6.3 mb	0.433	24.3 ± 2.7
K^+	7.37 ± 0.79 mb	0.522	3.85 ± 0.41
p	2.19 ± 0.31 mb	0.223	0.489 ± 0.069
ϕ	0.254 ± 0.067 mb	0.999	0.254 ± 0.067
Λ^0	0.885 ± 0.203 mb	0.176	0.156 ± 0.036
Ξ^-	0.141 ± 0.041 mb	0.527	0.0743 ± 0.0216

The extraordinarily good fit to a simple exponential in mass is somewhat of a surprise since it relies in no way on the significant amount of translational energy observed experimentally for these particles. There is also no hint of a distinction between Bose-Einstein statistics and Fermi-Dirac statistics. We do have good evidence that there is some Bose-Einstein interference between observed pion pairs in this experiment [21].

The best fit values for A (45.3±2.8 mb) and T (204±14 MeV) are remarkable for their apparent relation to other meaningful physical parameters. As we note in Section XV , if cross sections fall exponentially, the Uncertainty Principle suggests that $T = \hbar c/r_h$, where the hadronic radius is $r_h \approx 0.97 \pm 0.07$ fm. The value of $A = 45.3$ mb $\approx 0.721 \cdot (\pi \lambda\!\!\!^{-2}_{\pi})$ should be compared to the fact that the $\pi^{\pm}p$ cross sections [18] at the J=3/2, I=3/2 resonance saturate for a value given by

$$\sigma(\pi p) \approx 0.797 \cdot (\pi \lambda\!\!\!^{-2}_{\pi})(2J+1). \qquad (7)$$

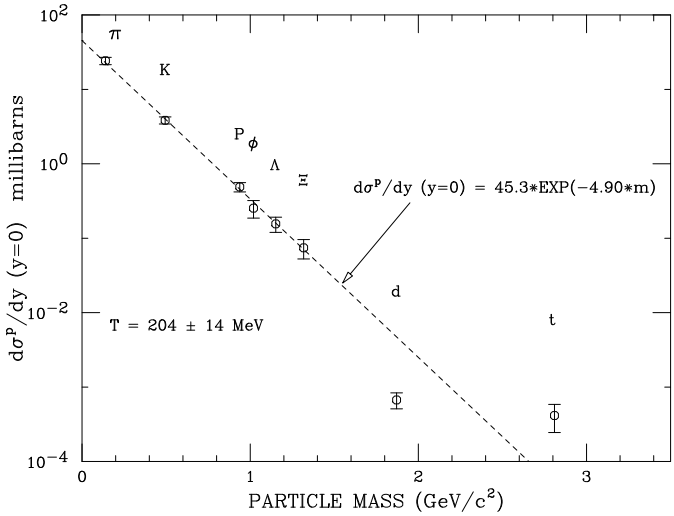

FIG. 4: Measured cross sections are scaled down to remove secondary contributions from decay of higher mass resonances and then divided by spin degeneracy $(2J+1)$ before plotting. The dotted line is a Boltzmann distribution in mass using $T = 204$ Mev obtained from a fit to the primary cross sections for the 6 elementary particles. The two nuclear cross sections per spin state are plotted to show the extent to which they do not appear to participate directly in this simple thermal model.

VII. EXTRAPOLATION TO HIGHER MASSES

If particle production as described by the above thermal model is valid for higher particle masses, then the thermal model can serve as a lower limit for presently unmeasured cross sections or it can be used as a standard measure for identifying unusually large cross sections.

Checking the validity of the thermal model at high mass values is difficult for two main reasons. One reason is that almost all event triggers at the large collider

detectors rely on finding particles with high p_t. The few cross sections which have been measured apply only to the highest portion of some incompletely known momentum spectrum.

Another reason is that detailed branching ratios like those we used to prepare Fig. 3 are unknown or unpublished, so that one cannot easily calculate a primary cross section. Only if one could find a particle like the ϕ meson (Fig. 3d) with negligible contributions from nearby mass resonances, would it be unnecessary to know detailed branching ratios for that particle.

We have attempted to make order-of-magnitude cross section estimates per spin state for four massive particles using reported data. These are plotted as X's without error bars in Fig. 5 for comparison with the extrapolated thermal model. Some calculational details of these estimates are outlined in the Appendix.

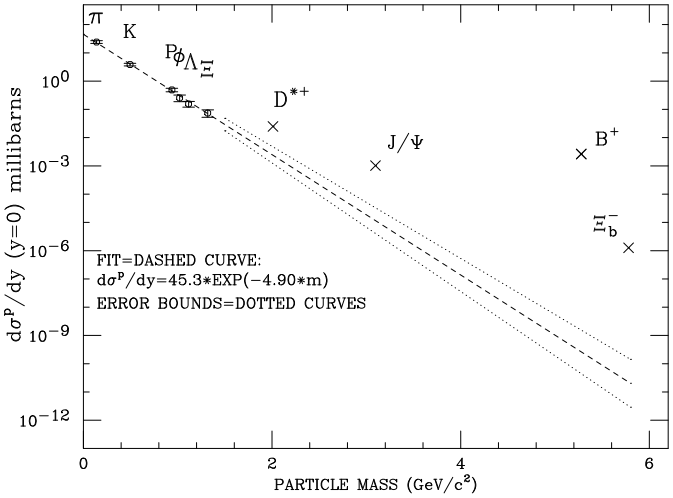

FIG. 5: The dashed curve is a fit to cross sections observed in this experiment. In the figure the curve is extrapolated to much higher mass values and is bounded by dotted curves which represent statistical errors for the fitted temperature.

An extrapolation of the fit to our six primary cross sections is shown as a dashed line in Fig. 5 bounded by dotted lines representing the slope errors for the fit. Although the higher mass cross section estimates in this figure have varying degrees of unreliability, they all lie above the expectations of thermal production, and the discrepancy tends to grow with increasing mass.

The D^{*+} cross section appears to be almost an order of magnitude above the thermal production expectations. There are very few examples of secondary decay contributions from nearby resonance decays into D^{*+} that are listed by the PDG [18]. Admixtures of B mesons are expected to decay as $B^{\pm o} \rightarrow D^{*+} + Anything$ 22.5% of the time [18], but the B^+ cross section alone is about an order of magnitude below the D^{*+} cross section.

If all secondary sources of D^{*+} can be accurately accounted for, it may eventually be possible to calculate a primary cross section that agrees with the thermal model. However, since the number of secondary sources tends to increase exponentially with mass [22], it may never be practical to isolate primary cross sections for the heavier particles.

The estimated J/ψ cross section is approximately two orders of magnitude above the thermal model prediction. There are 11 spin states of χ_{c1}, χ_{c2}, and $\psi(2S)$ which have significant decays (20% to 56%) into J/ψ. However, it seems unlikely that the primary thermal production of J/ψ is a source which is competitive with other constituent scattering sources.

Momentum distributions have been measured for D^{*+}, J/ψ, and B^+ production perpendicular to the colliding beams [23, 24, 25]. In the range of $6 < p_t < 20$ GeV/c the D^{*+} and J/ψ spectra fall off with a definite inverse power law ($d\sigma/dp_t \sim 1/p_t^5$). This is the same large p_t dependence observed in pion production at 90^0 for large $\sqrt{s}$ collisions [26]. Independence of $\sqrt{s}$ and particle mass are sufficient reasons to identify this common behavior as Feynman-scaling [27], which is typically associated with hard parton scattering [28]. However, the p_t dependence of the cross sections we have measured in this experiment is better represented by an exponential function up to 1.5 GeV/c for identified protons and up to 3.0 GeV/c for Λ^o's. At large particle masses where the thermal cross sections are expected to be very small, hard parton scattering may be the dominant production mechanism.

VIII. HADRONS FROM e^+e^- COLLISIONS

Although reliable cross section values for higher mass particles are not available for $p\bar{p}$ collisions, some have been measured in e^+e^- collisions. It would be interesting to learn if the thermal model in some way mediates hadron production in electron collisions. We have chosen to investigate this possibility by studying multiplicity fractions for charm particle production.

The multiplicity fraction f_h for a particle is the ratio of the inclusive cross section for producing the particle to the total cross section for producing hadrons: $f_h = \sigma^{incl}/\sigma^{hadron}$. Thus we treat multiplicity fractions for charm production in e^+e^- collisions in the same way as we treat inclusive charm cross sections resulting from hadron collisions. For example, the multiplicity fraction for D^+ production, $f_h(D^+)$, contains a primary component as well as secondary contributions from the decay of higher mass particles.

The PDG provides tables [29] of the total hadronic fractions f_h for a set of charm particles. Although data points are tabulated for collisions at $\sqrt{s} = 91$ GeV and $\sqrt{s} = 10$ GeV, we will focus on the data from $\sqrt{s} = 91$ GeV in an effort to achieve smaller errors. Values of f_h measured at $\sqrt{s} = 91$ GeV are listed for 6 charm particles in Table V and plotted in Fig. 6(a).

Because the production rates of b and c quarks in e^+e^- scattering are comparable in size at $\sqrt{s} = 91$ GeV (the Z^0 mass), the contribution of b quarks to the total hadronic

fraction of a charm particle can be substantial and must be subtracted in order to obtain the fraction contributed by c quarks,

$$f_c = f_h - f_b. \tag{8}$$

Fortunately it is possible to obtain f_b for a limited number of charm particles from a set of partial widths Γ tabulated by the PDG. [30] Using the partial width $\Gamma(b \to c)$ for a b-admixture to yield a charm particle c, one can calculate f_b directly.

$$f_b = \Gamma(b \to c) \times \Gamma(Z^0 \to b\bar{b})/\Gamma(Z^0 \to hadrons) \tag{9}$$

$$f_b = \Gamma(b \to c) \times (0.2163 \pm 0.0007), \tag{10}$$

where $\Gamma(Z^0 \to b\bar{b})$ and $\Gamma(Z^0 \to hadrons)$ are the partial widths for Z^0 decay into $b\bar{b}$ and hadrons respectively [31].

The first five values of f_c listed in Table V were obtained as outlined above. Errors for these values range from 5% to 30%. However, the last value, which is for J/ψ production, presents a special case because 95% of J/ψ particles produced at $\sqrt{s} = 91$ GeV come from the decay of B hadrons [32]. The error on the difference in Eq.(8) may be comparable to the difference itself.

One might consider associating f_c with the experimentally prompt component of J/ψ production at $\sqrt{s} = 91$ GeV, but the statistical accuracy on a direct measurement of prompt J/ψ production at this energy is poor [32]. Nevertheless, the prompt value at $\sqrt{s} = 91$ GeV is close to the total value [29] obtained with much greater accuracy at $\sqrt{s} = 10$ GeV (where b quarks are not produced). We have used this more accurate value for f_c in Table V for J/ψ production.

TABLE V: This table lists multiplicity fractions extracted from charm production in e^+e^- collisions [29]. Column 1 identifies the charm particle. Column 2 gives the experimentally observed fractions for charm particle production at $\sqrt{s} = 91$ GeV. Column 3 gives the fraction when contributions from b decays are removed. Column 4 gives the primary fraction after contributions from higher mass charm decays are also removed.

Name	f_h	f_c	f_c^p
D^0	0.454 ± 0.030	0.325 ± 0.031	0.0690 ± 0.0065
D^+	0.175 ± 0.016	0.125 ± 0.016	0.058 ± 0.008
D_s^+	0.131 ± 0.021	0.099 ± 0.022	0.033 ± 0.007
D^{*+}	0.194 ± 0.006	0.156 ± 0.007	0.0384 ± 0.0017
Λ_c^+	0.078 ± 0.017	0.057 ± 0.018	0.0057 ± 0.0018
J/ψ	0.0052 ± 0.0004	0.0005 ± 0.00005	0.000148 ± 0.000015

Our objective is to determine if the 6 observed values of f_h in Table V are consistent with the thermal model that describes hadron production in $p\bar{p}$ collisions. To do this we must correct f_c for contributions from secondaries of other charm decays. We can write f_c as a sum of contributions as follows.

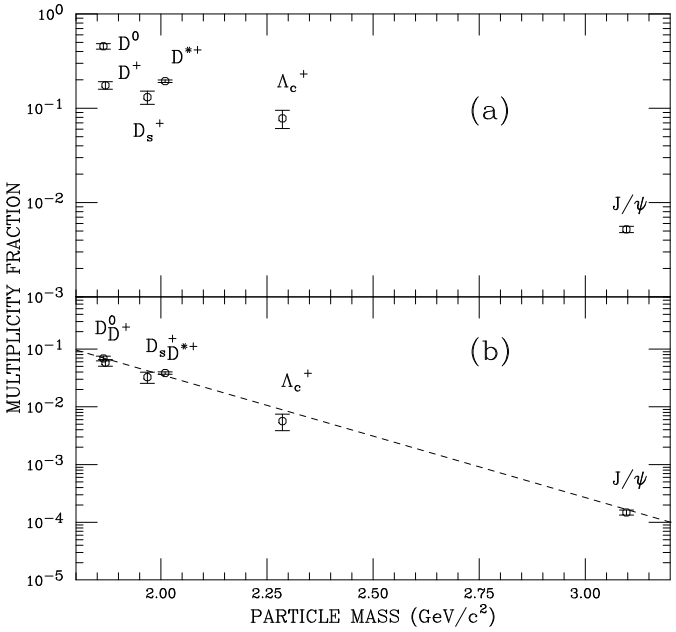

FIG. 6: (a) Observed hadronic multiplicity fractions at $\sqrt{s} = 91$ GeV [29] vs. charm particle masses. (b) Primary multiplicity fractions per spin state after correcting for secondary decay contributions. Dashed curve is an exponential $6.53 \times 10^2\, e^{-m/T}$, where m is particle mass and $T = 0.204$ GeV.

$$f_c = (2J_c + 1) f_c^p + \sum_i (2J_i + 1) f_i^p B_{ic} \tag{11}$$

In this expression f_c is the observed multiplicity fraction for charmed particle c. The primary fraction per spin state for particle c is f_c^p, and J_c is the spin of particle c. Similarly f_i^p is the primary fraction of particle i with spin J_i that contributes secondary decay products to the multiplicity fraction observed for particle c. B_{ic} is the branching fraction of particle i into particle c, and in some cases it is the result of a decay chain.

In the charm sector the branching fractions B_{ic} are sometimes poorly determined. We make use of data summarized in 2008 by the PDG [18]. For some particles branching fractions into hadrons are given as "seen" or "dominant". In order to obtain numerical estimates in these cases we make use of isospin symmetry, phase space ratios, and Clebsch-Gordon coefficients. Usually the most uncertain branching fractions are for higher mass particles which have smaller multiplicity fractions and thus contribute fewer secondaries.

To test for consistency we estimate the primary fragmentation f_i^p using the exponential fall off which we found for cross sections in $p\bar{p}$ collisions,

$$f_i^p = f_c^p e^{-(m_i - m_c)/T} = f_c^p \epsilon_{ic}, \tag{12}$$

where $T = 0.204$ GeV. After inserting this in Eq.(11), we can solve for f_c^p, the primary fragmentation fraction per spin state of charmed particle c.

$$f_c^p = \frac{f_c}{\left[(2J_c+1) + \sum_i (2J_i+1) B_{ic}\epsilon_{ic}\right]} \qquad (13)$$

This expression has two useful attributes. (1) Computation of f_c^p depends only on the measurement of one multiplicity fraction, f_c, and not on other measured fragmentation fractions and their possible experimental errors. This could be useful in identifying a single faulty measurement since there is no interdependency on other multiplicity measurements. (2) The primary fraction f_c^p can never be negative, which can happen if one "subtracts" secondary contributions using other measured fractions that have experimental errors and uncertain double counting in decay chains.

TABLE VI: Column 2 of this table lists sources of secondary particles that were used to correct the observed fractions for the particles in column 1.

Particle	Secondary Sources
D	$D^*, D_0(2400), D_1(2420), D_1(2430)$
	$D_2(2460), D_1(2640), D_{s1}(2536), D_{s2}(2573)$
D_s	$D_s^*(2112), D_{s0}(2317), D_{s1}(2460), D_{s1}(2536)$
D^*	$D_1(2420), D_1(2430), D_2(2460)$
	$D_1(2640), D_{S1}(2536)$
Λ_c	$\Sigma_c(2455), \Sigma_c(2520), \Lambda_c(2595), \Lambda_c(2625)$
	$\Sigma_c(2800), \Lambda_c(2880)$
J/ψ	$\chi_{c1}, \chi_{c2}, \psi(2S), X(3872)$

The sources used for secondary decay contributions are listed explicitly in Table VI. All of these sources have been limited to the charm sector since the earlier subtraction of f_b accounted for the contributions from B hadrons.

Six calculated primary multiplicity fractions per spin state, f_c^p, are listed in column 4 of Table V and plotted in Fig. 6(b). These were computed using Eq.(13) with f_c data from column 3 of Table V. The dashed line is a fit for normalization using $f_c^p = A\, e^{-m/0.204}$, which gives $A = 653 \pm 24$ with $\chi^2_{dof} = 2.8$. This could be considered a reasonably good fit, since the error bars in Fig. 6(b) simply employ the same percentages as those given for the observed multiplicity fractions, and no allowance is made for systematic inconsistencies among various experiments.

When corrections for all secondary decay contributions are completed, the D^0/D^+ isospin violation evident in Fig. 6(a) disappears in Fig. 6(b), which is encouraging since we did not use directly measured D^* fractions to bring about the agreement. This isospin symmetry violation (difference in multiplicity fractions) for the D^+ and D^0 is understood in terms of energy violation for decay of D^* into D^+ [33].

One can conclude that the six charm multiplicity fractions in Fig. 6(b) are consistent with a thermal production model. We have optimistically assumed that errors in the branching fractions B_{ic} are negligible. Since branching ratios for decays of higher mass particles are sometimes poorly determined, these errors in some cases could be significant.

We have also attempted this same analysis using e^+e^- multiplicity fractions tabulated entirely for $\sqrt{s} \approx 10.5$ GeV [29]. By working at that energy experimenters should have eliminated b-quark fragmentation from the data. Our analysis result at this lower value of $\sqrt{s}$ yields a fairly good description by $T = 204$ MeV for the non-strange charm particles, but there is a "strangeness suppression" of about a factor of two for D_s^+ and D_s^{*+} mesons which does not appear at $\sqrt{s} = 91$ GeV. This could be a physical effect that is related to the choice of a lower $\sqrt{s}$ or it could be the result of some systematic experimental error, such as a slightly incorrect Monte Carlo model.

IX. MODELS FOR PRIMARY CROSS SECTIONS

The scale factor for our cross sections ($\pi\lambda\!\!\!^{-2}_{\pi}$) has been a familiar feature since the discovery of the $\Delta(3,3)$ resonance, and the temperature (T) appears to be almost a trivial consequence of hadronic size and the Uncertainty Principle. Nevertheless, one would like to find a more fundamental description of particle production in high energy collisions that could give physical meaning to these and other observables.

In what follows we will examine several descriptions. The foremost requirement for each of these is that it must be compatible with the observed primary cross sections. In addition to that, a useful description should guide us to some reasonable approximation for the measured average transverse momentum $<p_t>$ of each studied particle. The *measured* value of $<p_t>$ is, of course, not that of the particles from primary production, since there is in general no experimental way to distinguish primaries from the secondaries of resonance decays. One can hope that the random nature of the decay process will have less effect on the average p_t than it will on the exact shape of the p_t distribution. We present some Monte Carlo calculations in Section XI that support this hope. Finally, a successful description should yield some gross approximation to the observed p_t spectra after making reasonable allowances for distortions by contributions from secondaries of resonance decays.

As we investigate descriptions, we will recognize the possibility that the final state of the particles may be different from the initial production state. That is, we consider cases where the final temperature may be different from the initial temperature as long as the particle ratios remain the same.

A. Hawking-Unruh Radiation

A recent approach to particle production has been to consider it as a consequence of Hawking-Unruh radiation [34]. In this description the rate R for the production of a particle of mass m is

$$R \propto e^{-m/a} \qquad (\hbar = c = 1), \tag{14}$$

where a is the particle acceleration. This is the result of a quantum mechanical tunneling calculation first used by Schwinger to describe pair production by an electric field [35]. Hawking later used this method to calculate the temperature of black holes, where the acceleration at the event horizon was considered to serve exactly as a temperature [36].

When applied to high energy experiments, the acceleration process is initiated by the particle collisions. Some estimates for the temperature are $T = Q_s/2\pi \approx 200$ MeV [34], $T = \sqrt{3\sigma/4\pi}$ [37], $T = \sqrt{\sigma/2\pi}$ [37]. Q_s is the "saturation scale" in the gluon saturation regime. In the last two expressions σ is the string tension between quarks in units of MeV^2. Our fit to the data with $T = 204$ MeV is in agreement with acceptable values of string tension.

It is important to note that the above estimates of acceleration do not have a mass dependence. A more recent version of this approach [38] introduces quark masses. The resulting temperatures then imply strangeness and charm suppression. In earlier sections we have shown there is no significant evidence to support suppression of strangeness or charm production in primary cross sections.

B. A Bootstrap Description

The bootstrap model was proposed by Hagedorn [22] after he first noted that the density of mass states known at that time increased almost exponentially with mass. A single state is defined as a particle or antiparticle with particular eigenvalues for mass, spin (J_z), and isospin (I_z). Frautschi [39] has written a paper that refines the bootstrap assumptions and concisely explains such a model and its consequences. The principal results are a limiting temperature T_0, sometimes called "the boiling point of matter", and a limiting analytic form for the density of states, $\rho(m)$, as a function of the mass m.

$$\rho(m) = c\, m^a\, e^{m/T_0} \qquad (a < -5/2). \tag{15}$$

Hagedorn has suggested a "smoothed" version of this expression which could be used at low masses or even at $m = 0$ [22, 40],

$$\rho(m) = c\, T_0^{3/2}\, (m_0^2 + m^2)^{-5/4}\, e^{m/T_0}. \tag{16}$$

Hagedorn expected values of $c = 5.5^{3/2}$, $m_0 = 500$ MeV, and $T_0 = 160$ MeV.

The inverse of this expression is so similar to the mass dependence of $d\sigma/dy|_{y=0}$ that we have tried fitting the cross section data with

$$\left.\frac{d\sigma^p}{dy}\right|_{y=0} = A\, T^{-3/2}\, (m_0^2 + m^2)^{5/4}\, e^{-m/T}, \tag{17}$$

where A and T are fittable parameters, and $m_0 = 500$ MeV is Hagedorn's choice of a smoothing parameter.

The results are shown in Fig. 7 with $A = 17.2 \pm 1.5$ mb/GeV, $T = 0.1397 \pm 0.0032$ GeV, and $\chi^2_{dof} = 0.30$. The parameters A and m_0 are strongly correlated and poorly constrained by the cross section data, which is why we accept Hagedorn's determination for m_0 without making it a free fitting parameter. We observe that $T_0 > T$, so that the cross section appears to decrease with increasing mass faster than the density of states increases.

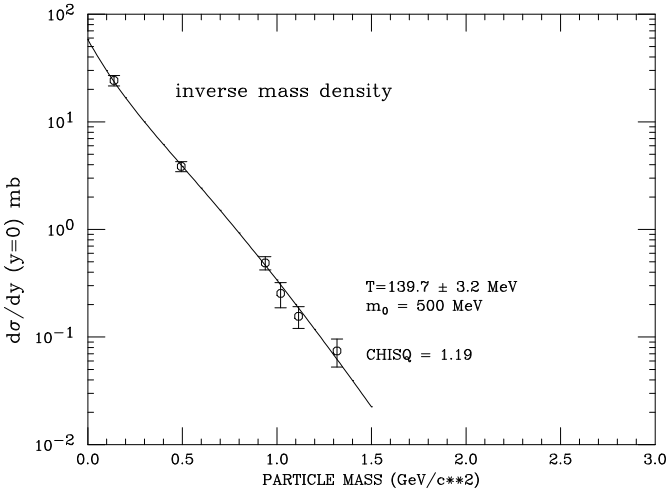

FIG. 7: The solid curve is a fit to cross sections observed in this experiment using the inverse of the mass density $\rho(m)$ suggested by the Hagedorn bootstrap model.

The use of this expression for the cross section suggests that to some extent we may observe an exponential decrease in $d\sigma^p/dy$ with increasing mass because we choose to measure only one of the many available states at mass m, whereas the number of available states increases exponentially with increasing mass.

C. A Gas Model

In this section we will explore the possibility that a relativistic gas model may describe the observed particle production cross sections. We make use of an expression for the number of particles per unit volume, dn, in the center of mass system given by [41]

$$dn \propto \frac{d^3\mathbf{p}}{[e^{(E-\mu)/T} \mp 1]}, \tag{18}$$

where T is the gas temperature and μ is a chemical potential. The volume element in momentum space, $d^3\mathbf{p}$, is given by

$$\begin{aligned} d^3\mathbf{p} &= 2\pi\, p_t dp_t\, dp_l \\ &= 2\pi\, p_t dp_t\, E\,(\frac{dp_l}{E}) \\ &= 2\pi\, p_t\, E\, dp_t dy \end{aligned} \tag{19}$$

The total energy of a particle is E. p_t and p_l are respectively components of its momentum transverse and parallel to the beam direction in the center of momentum system. The variable $y = (1/2)ln[(E + p_l)/(E - p_l)]$ is the rapidity. In our experiment $p_l \approx 0$. Thus one can use $E = \sqrt{p_t^2 + m^2}$ for the total energy of a particle of mass m and take $y = 0$.

In order to calculate a primary cross section a simple assumption is made that

$$\frac{d\sigma^p}{dy}\Big|_{y=0} = A\frac{dn}{dy}\Big|_{y=0}. \tag{20}$$

To obtain the cross section for any particle it then becomes necessary to evaluate the integral

$$\frac{dn}{dy}\Big|_{y=0} = \int_0^\infty \frac{p_t\, E\, dp_t}{[e^{(E-\mu)/T} \mp 1]}. \tag{21}$$

These integrals are done numerically. The second term in the denominator of the integrand should be -1 for bosons and +1 for fermions. In our applications we find that for masses above those of the kaon and pion the second term is insignificant, so that all of the calculations in this paper have actually used the boson form.

A first attempt to describe the primary cross sections of Table IV was made by assuming the chemical potential $\mu = 0$ for all particles and by fitting equations 20 and 21 to constants A and T. The result is the curve shown in Fig. 8.

Fitted values are $A = (3.69 \pm 0.71) \times 10^3$ mb/GeV^3 and $T = 0.1317 \pm 0.0038$ GeV. Unfortunately the χ^2 for this fit, $\chi^2 = 14.15$ for 4 degrees of freedom, is unacceptable. The main difficulty seems to be a failure to predict a large enough pion cross section. This difficulty can be addressed by selecting a suitable chemical potential.

From the thermodynamics of a system with k types of constituents, one knows that a change dU in the internal energy of the system can be written as [42]

$$dU = TdS - pdV + \sum_{i=1}^{k} \mu_i dN_i. \tag{22}$$

It should be possible to estimate a value for the chemical potential of a pion, μ_π, using a gedanken experiment which adds only one pion ($dN_\pi = 1$) to a system with temperature T and pressure p while arranging for entropy S and volume V to remain constant ($dS = dV = 0$). Then

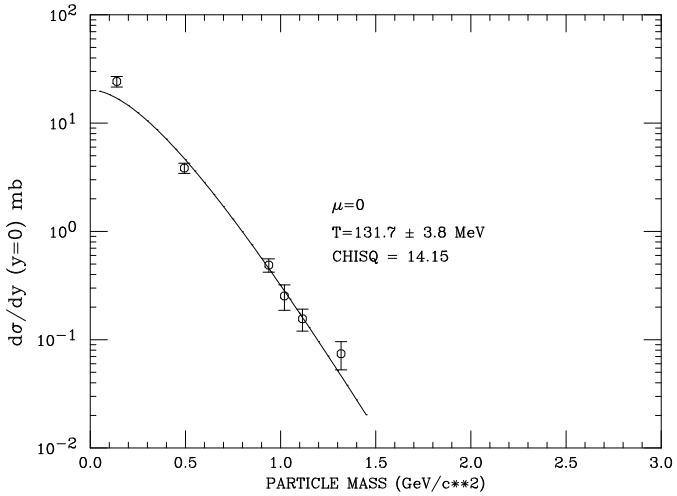

FIG. 8: The curve is a fit of the statistical gas model in Eq.(21) to the primary cross sections per spin state of 6 particles when the chemical potential $\mu = 0$ for each particle.

the chemical potential has a value $\mu_\pi = dU$. This suggests that $\mu_\pi = m_\pi$, but the relation with the pion mass must be such that $\mu_\pi < m_\pi$ if the integrand of Eq.(21) is to have no singular values.

Provided the system already contains constituent u and $\bar{d}$ quarks, one can imagine that dU need not supply the energy for existing quark masses. In that case we subtract existing quark masses [18] as below.

$$\begin{aligned} \mu_\pi = m_\pi - m_u - m_{\bar{d}} &= 0.1396 - 0.010 \\ \mu_\pi &= 0.1296 \quad \text{GeV} \end{aligned} \tag{23}$$

We have used this same value of μ in Eq.(21) for each of the 6 measured primary cross sections in order to fit for new values of A and T. This fitted curve can be compared to the data in Fig. 9.

The value of $A = (1.054 \pm 0.156) \times 10^3$ mb/GeV^3 and $T = 0.1371 \pm 0.0037$ GeV. The $\chi^2 = 4.35$ for 4 degrees of freedom is quite satisfactory from a statistical point of view.

The use of a common chemical potential μ for all the particles works best for fitting the pion data, and as we shall see later, it may influence the average kaon momentum in a beneficial way. It is not possible with the present data set to exclude the possibility that $\mu = 0$ for the heavier particles. On the other hand, it is easy to rule out the use of the thermodynamic arguments like Eq.(22) and Eq.(23) to determine a unique chemical potential for each mass because no reasonable fit to the cross sections was possible for that approach.

X. AVERAGE TRANSVERSE MOMENTA

Two significantly different temperatures are candidates for describing the production cross sections we have measured, T=204 MeV used with a simple exponential in the

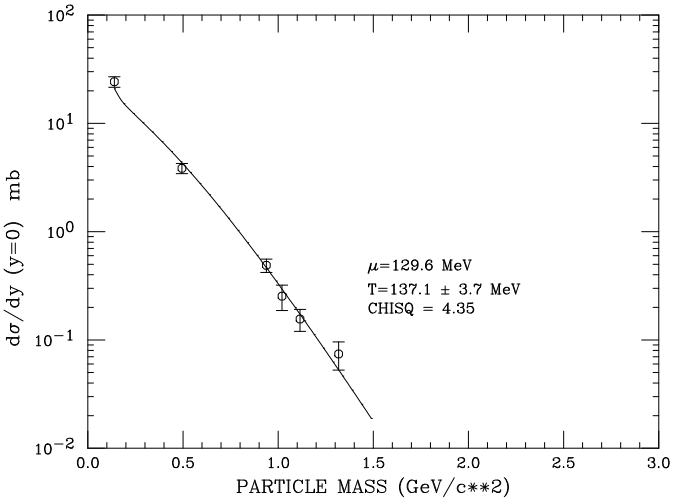

FIG. 9: The curve is a fit of the statistical gas model in Eq.(21) to primary cross sections per spin state when the chemical potential $\mu = 129.6$ MeV for each of the 6 particles.

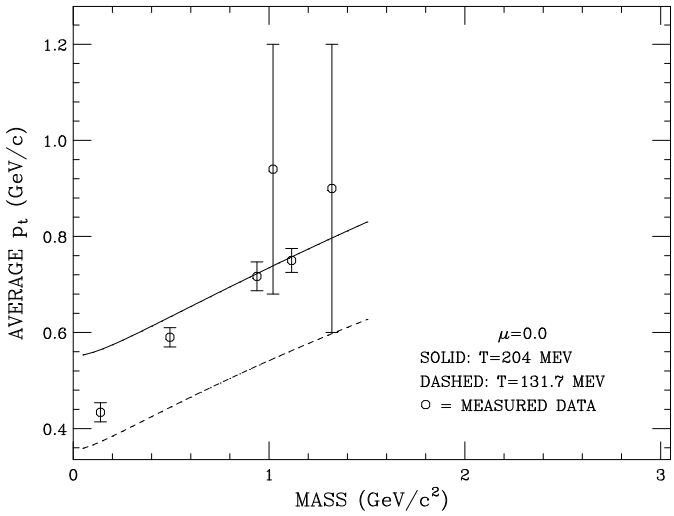

FIG. 10: The curves represent average transverse momentum expected from a Bose-Einstein distribution with chemical potential $\mu = 0$. The solid curve is for temperature $T = 204$ MeV and the dashed curve is for $T = 131.7$ MeV.

mass or T=137.1 MeV used in a relativistic gas model. We will first try to determine if either of these two temperatures is more appropriate for characterizing the measured values of average transverse momentum.

Consulting Eq.(21), we find that the relative transverse momentum spectrum at y=0 should be given by

$$\frac{dn}{dy\,dp_t}\Big|_{y=0} = \frac{p_t\,E}{[e^{(E-\mu)/T} \mp 1]}. \tag{24}$$

The average transverse momentum is then calculated for each mass value as

$$<p_t>= \frac{\int_0^\infty p_t(dn/dy\,dp_t)\,dp_t}{\int_0^\infty (dn/dy\,dp_t)\,dp_t}. \tag{25}$$

An initial calculation was done using chemical potentials $\mu = 0$. Curves of $<p_t>$ versus mass are plotted in Fig. 10 for T=204 MeV and T=131.7 MeV, the latter being slightly more appropriate for $\mu = 0$ as in the fit of Fig. 8.

In Fig. 10 it appears at first sight that the value of T=204 MeV has some amount of promise for being useful and that T=131.7 MeV is completely inappropriate. Neither curve recognizes the more pronounced decrease with mass in the experimental values of $<p_t>$ for the kaon and pion.

This last feature is improved by using the chemical potential $\mu = 129.6$ MeV. Fig. 11 compares use of T=204 MeV and T=137.1 MeV, the latter number being more relevant for the non zero value of μ as in Fig. 9. The higher temperature curve now comes closer to the measured values for the kaon and pion, but it is still well outside experimental error bars. The lower temperature curve remains unacceptable because of a nearly uniform displacement below the data points.

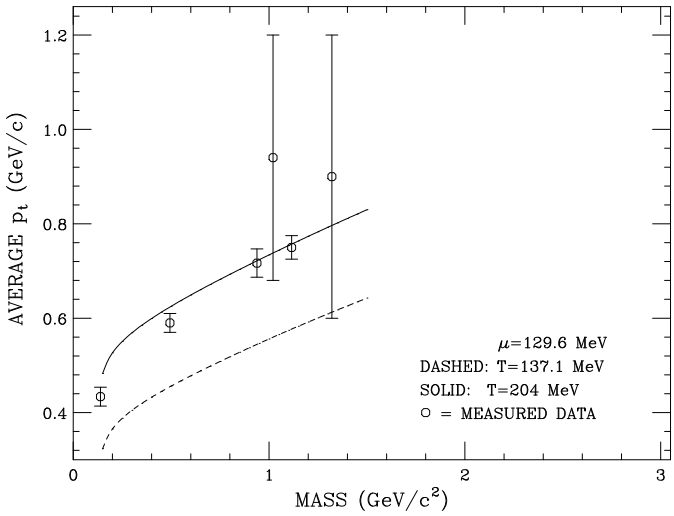

FIG. 11: The curves represent average transverse momentum expected from a Bose-Einstein distribution with chemical potential $\mu = 129.6$ MeV. The solid curve is for temperature $T = 204$ MeV and the dashed curve is for $T = 137.1$ MeV.

This displacement can be understood if one uses a suggestion made by Levai and Müller [20] which said that part of the transverse momentum may be due to the transverse flow of the gas as a whole. In order to calculate the effects of transverse flow it is advantageous to define a particle density 4-flow vector dN^ν. Within a constant factor this is given by [41]

$$dN^\nu(p) = d^3\mathbf{p}(\frac{p^\nu}{p^0})\frac{1}{[e^{(p^\nu U_\nu - \mu)/T} \mp 1]}, \tag{26}$$

where (p^ν/p^0) is the ν velocity component of particles in the infinitesimal group dN^ν. The particle distribution

function is here written in terms of an invariant $p^\nu U_\nu$. In this form it is sometimes called the Jüttner distribution [43, 44]. U_ν is the constant 4-flow velocity of the gas: $U_\nu = (\gamma_f c\ , -\gamma_f \mathbf{v_f})$, where $\mathbf{v_f}$ is the flow velocity and $\gamma_f = 1/\sqrt{1 - v_f^2/c^2}$. If the invariant is evaluated in the collision center of mass system for the case of a particle with momentum $\mathbf{p}$ parallel to the flow velocity $\mathbf{v_f}$,

$$p^\nu U_\nu = \gamma_f (E - \beta_f\, pc) = E', \tag{27}$$

where E' is the particle energy in the rest system of the flowing gas.

We obtain an expression which is needed for calculating cross sections by forming the invariant product

$$dN^\nu U_\nu = (\frac{d^3\mathbf{p}}{p^0}) \frac{p^\nu U_\nu}{[e^{(p^\nu U_\nu - \mu)/T} \mp 1]}. \tag{28}$$

When the flow velocity is zero, $v_f = 0$, the invariant product reduces to dn as used in Eq.(21). If the flow velocity is not zero and is parallel to the transverse momentum p_t, the invariant product becomes a more general expression for the invariant dn.

$$dn = \frac{p_t\, E'\, dp_t\, dy}{[e^{(E' - \mu)/T} \mp 1]} \tag{29}$$

E' is the energy of a particle in the rest system of the flowing gas and is calculated using Eq.(27).

The cross section data points are not effective in constraining values of the flow velocity $\beta_f = v_f/c$. Because of this we have estimated a value of β_f by fitting the 4 best measurements of $<p_t>$, those of the π, K, p, and Λ. Nevertheless it is still necessary to select a reasonably correct value of T to be used in Eq.(25) for computing $<p_t>$. We find a value of $\beta_f = 0.27 \pm 0.02$. The error is merely statistical and in no way reflects the systematic uncertainty caused by secondaries from resonance decays.

Some insight into the systematic error might be gained by observing how close the fitted curve in Fig. 12 comes to the $<p_t>$ measured for the proton, since the heavy mass of the proton causes recoil effects in decays to be less likely to shift average values of momenta. The curve is well within the statistical error on the measured value of $<p_t>$ for the proton.

The curve in Fig. 12 was obtained using $T = 131.5 \pm 3.4$ MeV. This is the temperature obtained if one fits the primary cross sections using Eq.(29) with $\beta_f = 0.27$. Thus the cross section fit and the β_f fit are consistent. For the cross section fit the normalizing constant (Eq.(20)) is $A = 600 \pm 86$ mb/GeV^3 and the $\chi^2 = 3.57$. The fitted curve using these values is imperceptibly different from that shown in Fig. 9.

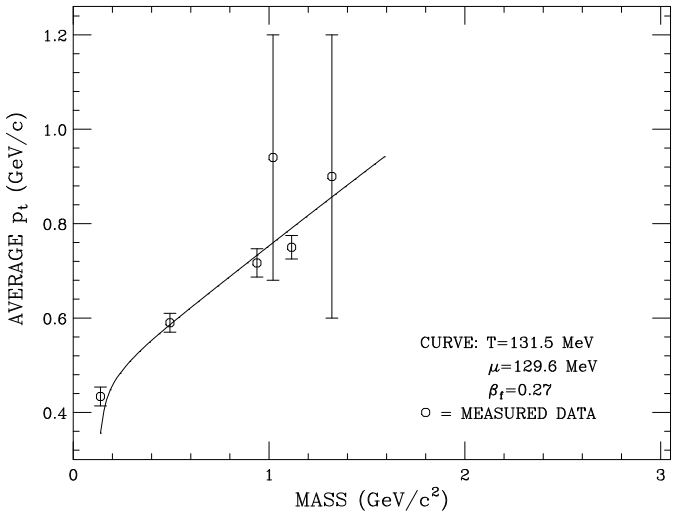

FIG. 12: The solid curve represents average transverse momentum expected from a Jüttner distribution with $T = 131.5$ MeV and chemical potential $\mu = 129.6$ MeV when momenta are boosted by a transverse flow with $\beta_f = 0.27$.

XI. TRANSVERSE MOMENTUM SPECTRA

Since the experimental p_t spectra of the particles are a mixture of primary particles and resonance decay products, it is a challenge to find a useful means of comparing them to the statistical predictions for primary particle production. The curves in Fig. 13 and Fig. 14 are statistical model predictions for primary p_t spectra of pions, kaons, and protons. Because these particle cross sections vary by an order of magnitude, the vertical scales for the curves have all been renormalized arbitrarily to fit in the same plot. Experimental data points have also been renormalized in order to help in making comparisons of data with model predictions.

Figure 13 compares data points with a model that has T=204 MeV and a chemical potential $\mu = 129.6$ MeV. Data points are cut off sharply at low momentum by absorption in the spectrometer material. The kaon and proton data are not extremely different from the predicted primary curves, but the pion data points are noticeably more condensed at low p_t than this model predicts for the primary pions.

Figure 14 compares data points with a model that has T=131.5 MeV, a chemical potential $\mu = 129.6$ MeV, and a transverse flow velocity $\beta_f = 0.27$. All three particle spectra are similar to model predictions in an encouraging way.

The influence of resonance decay products on the experimental p_t spectra is perhaps more complex than one might initially guess, especially for the spectrum of the much lighter pions. We have examined spectra from the production and decay of two "typical" resonances in our spectrometer using a Monte Carlo program. The program generates particles at T=204 MeV using no chem-

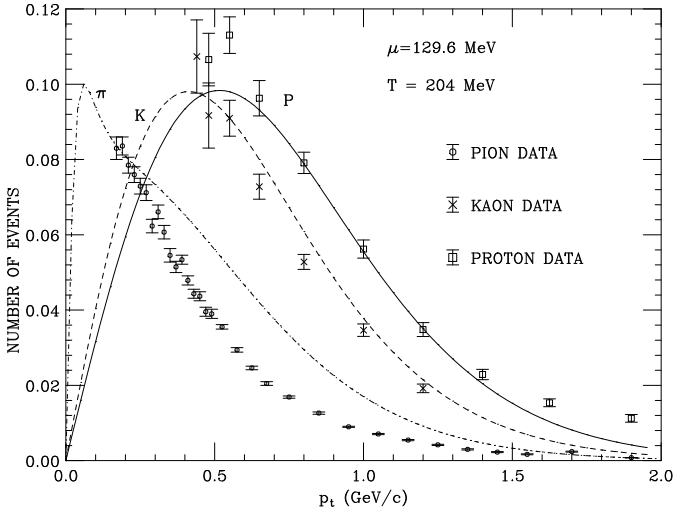

FIG. 13: The curves represent transverse momentum distributions for pions, kaons, and protons as expected from a Bose-Einstein distribution with temperature $T = 204$ MeV and chemical potential $\mu = 129.6$ MeV. Normalization was arbitrarily chosen to fit all three curves within the plot. Data points for the 3 particles were also normalized to facilitate comparisons with the 3 curves.

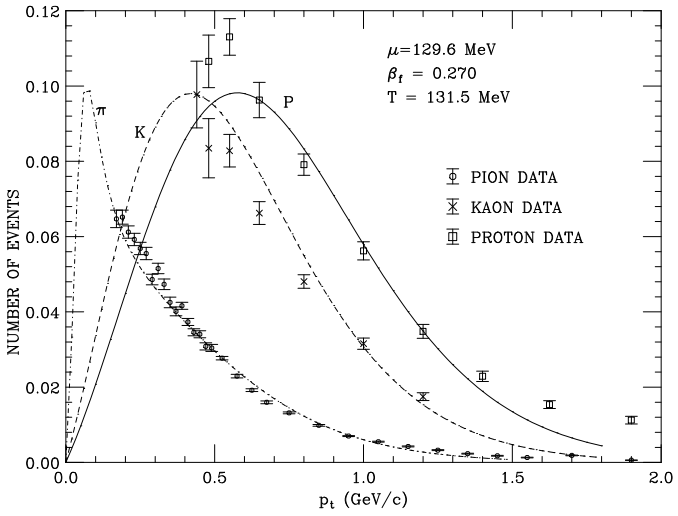

FIG. 14: The curves represent transverse momentum distributions for pions, kaons, and protons as expected from a Bose-Einstein distribution with temperature $T = 131.5$ MeV, chemical potential $\mu = 129.6$ MeV, and transverse flow velocity $\beta_f = 0.27$. Normalization was arbitrarily chosen to fit all three curves within the plot. Data points for the 3 particles were also normalized to facilitate comparisons with the 3 curves.

ical potential and assumes a flat rapidity distribution. Experimental acceptance cuts and magnetic field are included in the analysis, but absorption effects are ignored. For pion sources the typical resonance is chosen to have a mass $M^* = 1.3$ GeV and a decay mode $M^* \rightarrow p+\pi$. For proton sources the typical resonance is assumed to have a mass of $M^* = 1.6$ GeV and a decay mode of $M^* \rightarrow p+\pi$. The histograms in Fig. 15 show the Monte Carlo spectra. The *average* p_t values for the Monte Carlo proton and pion spectra are quite close to the experimentally measured values.

The shape of the pion spectrum shows a surprising peak at low momentum. Much of this peak comes from M^* resonances initially directed into the hemisphere opposite our detector. Backward pions from the decay of this resonance pass through the aperture of the detector and are processed as very low momentum pions. A small bump seen at $p_t \approx 250$ MeV/c in the experimental pion data might be associated with such an effect.

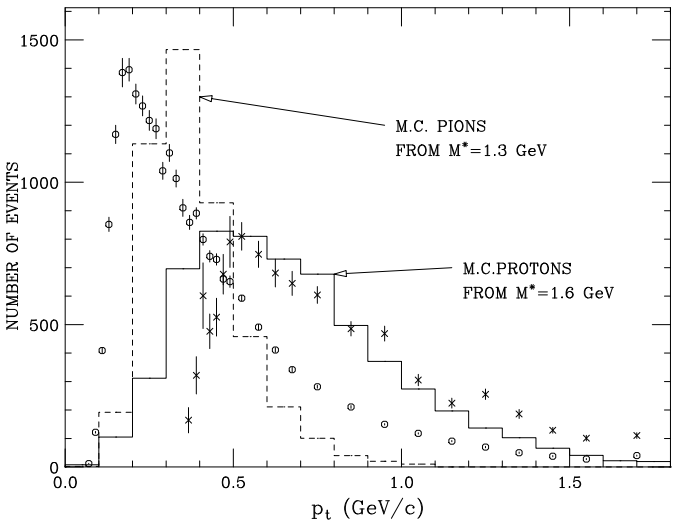

FIG. 15: Histograms are Monte Carlo generated distributions using a gas with $T = 204$ Mev. Dashed histogram represents pions from decay of $M^* = 1.3$ GeV to πp. Solid histogram represents protons from decay of $M^* = 1.6$ GeV to πp. Overall normalization is arbitrary. Data points are normalized to give areas comparable to the histograms for comparison purposes.

XII. LUMINOSITY AND TRIGGER ISSUES

There are two methods used to calculate the luminosity of a bunch crossing. One is the "machine method" and the other is the "cross section method". The machine method consists of first measuring and estimating properties of the particle bunches and the particle accelerator and then using these to calculate luminosity from first principles [11]. The cross section method counts the number of events from a beam crossing that result from a particular process and uses the known cross section for that process in Eq.(1) in order to calculate the luminosity. Once the luminosity is determined, all other cross section measurements are reduced to event counting experiments.

When we first began to evaluate cross sections for the 1988-1989 Tevatron run, the most accessible luminosities

were machine calculated values for which the data were posted at approximately two hour intervals by the accelerator operators. We have used these same machine luminosities [11] to calculate all cross sections presented in this paper.

The trigger used to collect the data which we present from this experiment was designed to select non-diffractive (nd) events. Therefore a cross section computed for this trigger, σ_{trig}, should closely approximate the best known value for the non-diffractive cross section, σ_{nd}.

Our primary trigger (PT) was typical of those used with collider detectors. It required a triple coincidence between far upstream and far downstream counters (BB) and the bunch crossing time T0. This coincidence was supplemented by time based vetoes to eliminate beam-gas events from halo and satellite bunches. Events selected by the PT trigger are called non-single-diffractive (nsd), because elastic (el) and single-diffractive (sd) events are effectively elimnated by it. Since our highest luminosity was around $2 \times 10^{28}\,\mathrm{cm}^{-2}\mathrm{sec}^{-1}$ (about two orders of magnitude below that of CDF), an interaction occured in about every 200 bunch crossings, and there was little need to consider cases where two sd events in the same bunch crossing could fake one nsd event.

The trigger (S1) used for collecting data reported in this experiment made use of the PT trigger described above in coincidence with a "track" in the spectrometer arm. A track was defined by requiring drift chamber hits in at least 3 of 4 possible planes both before and after the analysis magnet. This requirement of a spectrometer track near zero rapidity effectively eliminated double-diffractive (dd) events from the event trigger (S1).

TABLE VII: This table contains cross sections used to check our machine-derived luminosity against the more commonly used cross-section-derived luminosities. Column 3 gives sources for the cross sections listed in column 2.

Cross Section	Value (mb)	Source
σ_{trig}	41 ± 6	[6]
σ_{dd}	4.43 ± 1.18	[45]
σ_{sd}	9.46 ± 0.44	[46]
σ_{inel}	59.3 ± 2.3	[47]
σ_{nd}	45.4 ± 2.6	[45],[46],[47]

The first row of Table VII gives the cross section of the S1 trigger as computed using machine-determined luminosity for the C0 intersection, $\sigma_{trig} = 41 \pm 6$ mb. We should compare σ_{trig} to the non-diffractive cross section σ_{nd} as derived from cross-section-determined luminosities given in Table VII.

$$\sigma_{nd} = \sigma_{inel} - \sigma_{dd} - \sigma_{sd} = 45.4 \pm 2.6\,\mathrm{mb}. \qquad (30)$$

In this calculation we have used an average value for σ_{inel} which was adopted by the CDF and D0 collaborations for defining cross-section-determined luminosities [47]. Our machine-determined σ_{trig} is about 10% lower than the cross-section-determined σ_{nd}, but the two values agree within the errors. Should one ever choose to compare cross sections in this paper with those published by CDF or D0, then it might be desirable to shift one set or the other systematically by 10%.

It may be interesting to note that increasing all of our absolute cross sections by 10% would make the scale factor for our cross section fit agree almost exactly with that for πp scattering in Eq.(7).

XIII. ENERGY DEPENDENCE

Much can be learned about the properties of the thermal state by considering the production properties of the ϕ meson. As one can see from Fig. 3(d), there are negligible contributions to the inclusive ϕ cross section by secondaries from higher mass decays. The ϕ cross section at y=0 *is* essentially a primary cross section. If the same thermal production mechanism prevails in other experiments, then a measurement of the phi cross section in those experiments will allow a comparison of scales among experiments. The decay of the ϕ into lepton pairs and kaon pairs means that most experiments are equipped with a simple trigger which can record its presence.

Absolute cross sections at collider energies are rarely reported, but we are able to plot two additional values of $d\sigma/dy|_{y=0}$ for ϕ mesons in Fig. 16 as a function of s [48] . The lower energy cross sections are for pp collisions, and the highest energy one is our value at $\sqrt{s} = 1800$ GeV for $\bar{p}p$ collisions.

We have observed evidence for the thermal state only in collisions with the potential for annihilation ($\bar{p}p$ and e^+e^- initial states). The similarity of the pp and $\bar{p}p$ cross sections for ϕ mesons shown in Fig. 16 suggests that the origin of the thermal state may be in the interaction of gluons, which are common components of both protons and antiprotons.

An inelastic cross section such as the total cross section for ϕ production might be expected to have an energy dependence which is bounded by some relation like the Froissart limit [49], $\sigma_{tot}(\phi) \propto \ln^2 s$. To the extent that inclusive cross sections have a flat rapidity distribution for $|y| < y_{max}$, we can write

$$\sigma_{tot}(\phi) \simeq 2\, y_{max} \frac{d\sigma}{dy}\Big|_{y=0} \simeq \ln(s/m^2)\, \frac{d\sigma}{dy}\Big|_{y=0}.$$

In this case it seems likely the ϕ cross section at y=0 would respect a reduced Froissart limit of $d\sigma/dy|_{y=0} \leq \ln s$.

In Fig. 16 we have plotted best fits to

$$\frac{d\sigma}{dy}\Big|_{y=0} = \text{constant} \qquad (= 0.58 \pm 0.07\ \text{mb})$$

and

$$\frac{d\sigma}{dy}\Big|_{y=0} = A\, \ln(s/s_0) \quad (= 0.039 \pm 0.005) \cdot (\ln(s/m_\pi^2)\ \text{mb}),$$

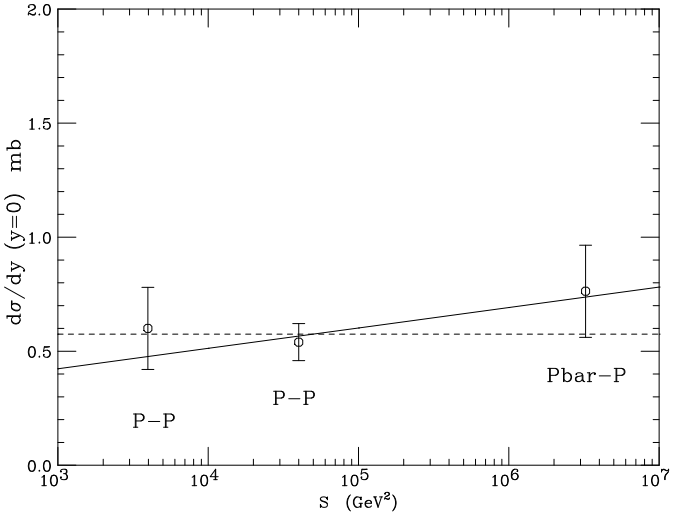

FIG. 16: Cross section $d\sigma/dy$ at y=0 for inclusive ϕ meson production is plotted vs. s, the square of collision energy. Cross sections show very little dependence on either energy or an annihilation option.

where s_0 is an energy scale factor to which fits are insensitive. We have chosen s_0 to be the square of the pion mass.

The $\ln s$ fit has a $\chi^2 = 0.59$, and the constant cross section fit has a $\chi^2 = 1.1$. Both possibilities are acceptable for 2 degrees of freedom. The data are consistent with a constant ϕ cross section or a slight increase with energy near a Froissart bound.

XIV. NUCLEAR CROSS SECTIONS

Although one can see in Fig. 4 that the two nuclear cross sections do not fit the thermal model well, they seem to exhibit a tendency to be in the neighborhood of the dashed curve that describes the model. The cross section per spin state for deuterium is a factor of 5.0 below the dashed curve, and the cross section per spin state for tritium is a factor of 8.7 above the dashed curve. It should be mentioned that these plotted points are estimates of the cross sections and not direct measurements. We should ask if the estimate for the deuterium cross section could be larger or if there might be a reason for the tritium cross section to appear so large.

The invariant cross sections, $(1/\pi)d^2\sigma/dydp_t^2$, for d^+, d^-, and t^+ were measured directly in a very limited range of p_t, but values for the integrated cross section $d\sigma/dy|_{y=0}$ had to be obtained without benefit of fully measured distributions of transverse momentum. The published estimates for deuterium and tritium were made using variations of a Boltzman momentum distribution which had adequately fit p_t spectra for K^- and $\bar{p}$ produced at $\sqrt{s} = 1.8$ TeV. Systematic errors were assigned based on the results of these variations.

The tritium cross section was based on 8 events satisfying experimental cuts. Only one possible anti tritium event was observed. Anti tritium is more heavily absorbed by the spectrometer material, but the recording of events was heavily prescaled by total multiplicity, sometimes as much as a factor of 26, so at this level of statistics it is only suspicious that there are not more anti tritium event candidates observed.

There are two reasons to consider why the tritium cross section plotted in Fig. 4 might be higher than expected. The first reason is that the observed tritium nuclei might not originate from the $p\bar{p}$ collisions. They might come instead from secondary interactions in the wall of the 2 mm thick aluminum beam pipe.

Approximately 2×10^7 particles entered the spectrometer arm during the experiment. Some of these in principle could have ejected a tritium nucleus from aluminum in a quasi elastic process such as

$$\pi^+ + {}^{27}Al \rightarrow \pi^+ + {}^{3}H + {}^{24}Mg\,, \qquad (31)$$

where ${}^{24}Mg$ is a spectator nuclear fragment. Using only this process, we find $\sim 12\%$ of the spectrometer particles have momentum high enough to produce the ${}^3H$ candidates we observe.

Spallation experiments have reported total cross sections of 27 mb for producing ${}^{24}Mg$ using protons with momentum of 1.2 GeV/c [50]. In no case have we found a published rate for ${}^3H$ production in a spallation experiment, although some might have had the ability to observe it. Much of the production of light masses is expected to come from a low energy evaporation process after the initial impact. However, if *all* of the 27 mb cross section for producing ${}^{24}Mg$ proceeds by Eq.(31) with ${}^3H$ in the forward direction, then there would be 800 tritium candidates in the spectrometer. If ${}^3H$ fragments exist in such numbers, it cannot be safely assumed that all of these would be eliminated by the vertex cuts we used.

There is a second reason the tritium point in Fig. 4 might appear too high. It could be that there are more contributing states to the cross section than the $(2J+1)$ spin states we assumed. The estimated cross section was divided by only $(2J+1)$ spin states before plotting.

Some evidence exists that well defined "nuclear" states exist in which one of the usual nucleons is replaced by a particle resonance. The best established examples of this can be found in the Λ^0 hyperfragments, where the Λ^0 lives long enough to give a distinctive decay signature in a detector. A collection of old data in reference [51] lists 12 hypernuclei ranging from ${}^3H_\Lambda$ to ${}^{13}C_\Lambda$ and tabulates their binding energies along with some observed decay modes. More recentlly high resolution spectrometers [52] have resolved excited energy levels for the bound Λ^0 in heavier nuclei. For ${}^{89}Y_\Lambda$ energy levels for s, p, d, and f Λ^0 orbitals have been resolved.

If N^* resonances can also be bound in nuclei, there might be many modes which would contribute to the observation of ${}^3H$ production in $p\bar{p}$ collisions. Although there seem to be no experiments designed to explore this

notion, one can find some indication of it. Inelastic cross sections for pions on tritium peak at a pion energy around 140 MeV [53], suggesting the formation of $\Delta(1232)$, and final state particle ratios in $\pi^{\pm}$ collisions with ${}^3H$ and ${}^3He$ are consistent with dominance by the Δ baryon resonance [54].

XV. LITTLE BANG NUCLEOSYNTHESIS

The Little Bang collision as observed in this experiment takes place in approximately 10^{-26} seconds as the Lorentz contracted disks of the proton and antiproton pass through each other. Interfering pions continue to be emitted [21] from the vicinity of the collision for times $\sim 10^3$ longer than the collision time, since the measured size of the emission volume has a "radius" of approximately 1 fm, somewhat larger than this in the longitudinal direction than in the transverse direction. Slightly larger emission dimensions are correlated with larger multiplicities of produced hadrons.

Several estimates [21, 55] have been made of the energy density in the emission volume at the time of hadronization. The values reported are sensitive both to the models used and the fraction of observed final state particles assumed to originate from the emission volume. Energy densities obtained range from ~ 4 to ~ 60 times that of a proton.

Primary cross sections per spin state for the light hadrons decrease with mass according to a Boltzmann distribution having a characteristic temperture $T = 204$ MeV. See Fig. 4. We can understand this temperature in a qualitative way if we assume that the collision deposits energy into a volume of hadronic size at the limit of the Uncertainty Principle. In that case $\Delta E\, c\Delta t = \hbar c$, where ΔE is the energy deposited and $c\Delta t$ is a characteristic hadronic radius r_h.

$$\Delta E = \hbar c / r_h \tag{32}$$

In the Uncertainty Principle ΔE is the measure of the drop-off energy of a probability function. For a Boltzmann distribution we can identify ΔE with T [56].

$$T = \hbar c / r_h \tag{33}$$

If all produced hadrons share the same radius r_h, then T is a constant which can be found experimentally. A value of $T = 204 \pm 14$ MeV implies a hadronic radius $r_h = 0.97 \pm 0.07$ fm. In some sense r_h has to be an average radius.

In this experiment we observe the production of deuterium and anti deuterium nuclei. The radius of a nucleus does not fit comfortably inside a hadronic radius, so its production must wait for the volume to expand to a larger radius $r > r_h$. According to Eq.(33) a larger radius will imply a correspondingly lower temperature and a smaller cross section than does the smaller radius of a hadron having the same mass as the nucleus.

Assuming a nuclear volume increases as the number of constituent hadrons, A, we can write an effective nuclear radius r_A as

$$r_A = r_h\, A^{1/3}. \tag{34}$$

The temperature for nuclear production becomes $T_A = \hbar c / r_A$, and the cross section in millibarns per spin state for producing a nucleus A becomes

$$\left.\frac{d\sigma(A)}{dy}\right|_{y=0} = 45.3\, e^{-m_A/T_A}. \tag{35}$$

Normalization at 45.3 mb fixes the primary proton cross section at the value previously used with $T = 204$ MeV.

A dashed curve in Fig. 17 plots the locus of nuclear cross sections per contributing state as predicted by Eq.(35). The experimental estimates for the d and $\bar{d}$ cross sections agree fairly well with the prediction of a modified temperature for nuclear production, whereas the experimental estimate of the ${}^3H$ cross section becomes 4×10^3 times larger than the dashed curve.

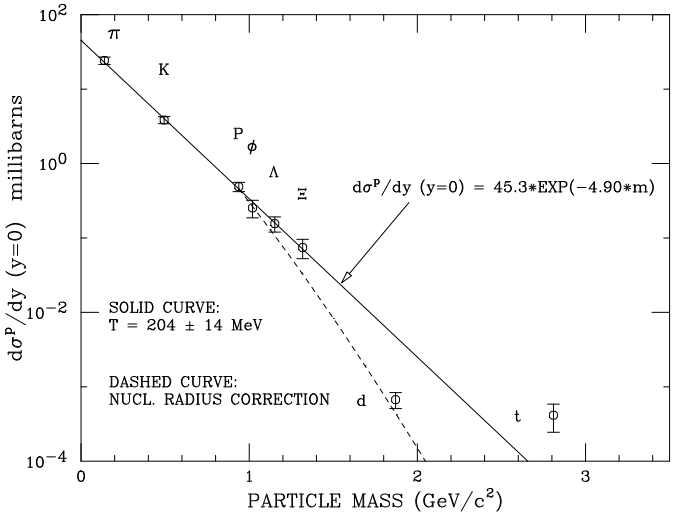

FIG. 17: Primary cross sections per spin state are compared to a Boltzmann distribution in mass for a temperature of $T = 204$ Mev (solid curve) and to a distribution modified to accomodate the radius of each individual nucleus (dashed curve).

Nuclear cross sections decrease so rapidly with mass according to Eq.(35) that only the lightest nuclei might be detected at colliders. Table VIII lists predicted production rates relative to $\bar{p}$ rates for several light elements. Based on our observation of 19 anti deuteron

events at $\int \mathcal{L}dt = 5.52 \pm 0.81\, nb^{-1}$, we estimate that at $\int \mathcal{L}dt = 2100\, pb^{-1}$ the CDF detector at the Tevatron could observe $\sim 3.6 \times 10^9$ anti deuteron events and ~ 27 anti ^4He events, provided there is no prescaling of the event triggers such as was used in our experiment. This estimate allows for the increased geometrical acceptance of the CDF detector but not for other detector specific features.

TABLE VIII: The production rate of a light nucleus relative to the production rate of antiprotons is calculated using the temperature model of Eq.(35). J_A is the nuclear spin, and A is the mass number of the nucleus. Spin degeneracies are included in the calculation of the rate ratio R.

Nucleus	A	J_A	$R = N_A/N_p$
^1H	1	1/2	1.0
^2H	2	1	1.38×10^{-3}
^3H, ^3He	3	1/2	2.27×10^{-7}
^4He	4	0	1.04×10^{-11}
^6Li	6	1	2.52×10^{-20}
^7Li	7	3/2	3.62×10^{-25}

If nuclei are really formed in nucleon-nucleon collisions, it should be relatively easy to verify the fact with suitable triggers in conjunction with one of the high resolution detectors that currently exist. It would be essential to require that the instrumentation not saturate on pulse heights up to 10X-20X minimum ionization. The high statistics expected for the lightest nuclei (^2H, ^3H, ^3He) would permit one to study the extent to which they are produced in pairs or to put limits on the equality of nuclear and antinuclear cross sections. Because a temperature of $T = 204$ Mev also seems to organize the hadron production cross sections from e^+e^- collisions, it may be useful to search for nuclear production in those data sets as well.

Little Bang Nucleosynthesis (LBN) would seem to be quite different from Big Bang Nuleosynthesis (BBN) [57]. BBN begins with a large net baryon number, but LBN begins with zero net baryon number, initiated perhaps by annihilation or by gluon-gluon interaction. Electrons and photons participate in BBN in a large way, but there is little evidence for either of these in LBN (see section IV). In BBN nuclei are formed at temperatures comparable to nuclear binding energies. Nuclei from LBN appear to be formed somehow in an environment with temperatures that are many times larger than nuclear binding energies.

Fig. 18 has been included here to illustrate the extent to which LBN fails to reproduce the relic cosmic abundances that BBN accounts for so well [57]. The ratio of cosmic abundances relative to hydrogen have been divided by (2J+1) for plotting. Nuclear curves from Fig. 17 have been inserted into the figure for comparison.

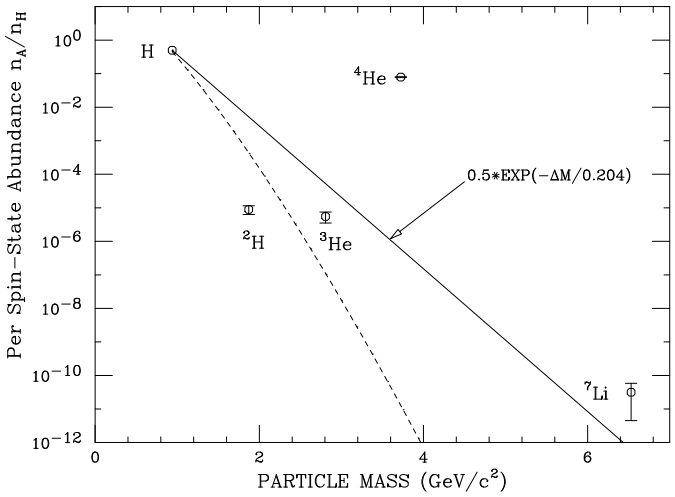

FIG. 18: Plotted points are relic cosmic abundances of ^2H, ^3He, ^4He, and ^7Li relative to hydrogen [57] after dividing each ratio by $(2J + 1)$. Variations of the Big Bang Nucleosynthesis model strive to reproduce these data points. The solid curve when used with $\Delta M = m_A - m_p$ has the slope for $T = 204$ MeV, which fits elementary particle production in this paper. The dashed curve represents a temperature modification which might accomodate nuclear size.

XVI. CONCLUSIONS

This paper has presented 9 absolute cross sections $(d\sigma/dy|_{y=0})$ for particle production at 90^0 to colliding p and $\bar{p}$ beams with $\sqrt{s} = 1.8$ TeV. One of these cross sections is for photon production. Two are for nuclear production. The remaining six are for light elementary hadron production.

The six hadron cross sections were corrected for secondary contributions from decays of higher masses in order to produce a set of six primary cross sections. When the primary cross sections are divided by the spin degeneracy $(2J + 1)$ of individual particles, we learn that the primary cross sections per spin state precisely follow an exponentially decreasing distribution in particle rest mass with a temperature $T = 204 \pm 14$ MeV. By summing over all spin states, one finds the total primary cross section for a particle of specified charge, spin J, and rest mass m is given by

$$\frac{d\sigma^p(\text{tot})}{dy}\Big|_{y=0} = 0.721 \cdot (\pi \lambda\!\!\!^{-2}_{\pi})(2J+1) \cdot e^{-m/T}. \quad (36)$$

Using an argument based on the Uncertainty Principle, we set $T = \hbar c/r_h$, where r_h is a hadronic radius given by $r_h = 0.97 \pm 0.07$ fm. For nuclear production we replace r_h by $r_A = r_h\, A^{1/3}$ and find a temperature T_A. When T_A is used in Eq.(36), it yields an acceptable value for the anti deuteron cross section.

This purely thermal production mechanism exhibits no significant strangeness suppression, implying that exper-

imentally observed strangeness suppression is entirely explained by contributions from decay products of higher masses. As discussed in section IV, we were unable to observe any primary production at the photon and electron masses, so the thermal mechanism is probably relevant only for strongly interacting particles.

It appears there may be two temperatures that are useful in describing the entire particle production process. The temperature T=204 MeV precisely describes the primary particle ratios in the initially produced state, and a temperature T=132 MeV describes the momentum distributions in a final decay state in which pions have a uniquely low momentum. An exothermic transition between the production state and decay state might account for a transverse flow velocity of $\beta_f = 0.27$. The average kinetic energy per particle associated with this transverse flow is ~ 20 MeV, and thus it is not a trivial amount.

It is possible to observe the thermal production mechanism in $p\bar{p}$ collisions at 90^0 (y=0) because of its dominant cross sections in the low mass region. For the production of masses in or above the charm sector there is evidence that other mechanisms such as parton scattering become dominant. The dominance may extend to many orders of magnitude at the highest particle masses.

We have examined cross sections for hadron production in the charm sector by e^+e^- collisions using published values of multiplicity fractions. To the degree that decay branching ratios are well known, we find that primary e^+e^- multiplicity fractions also follow a Boltzmann distribution in mass for a temperature $T = 204$ MeV. There is no significant evidence for strangeness suppression in the charm sector examined.

Since the ϕ meson is essentially a primary particle with negligible secondary contributions, one can possibly gain some insight into the origin of the thermal mechanism by studying ϕ production. The ϕ cross section at 90^0 is consistent with being the same for pp and $p\bar{p}$ collisions over a range of center of mass energies that vary by a factor of ~ 30. This may suggest that gluon interactions rather than annihilations are the essential source of the thermal production.

XVII. ACKNOWLEDGMENTS

We would like to thank V. Barger, C. Goebel, T. Han, and S. Dasu for helpful discussions. We are also indebted to Matt Herndon for answering our numerous questions about the CDF detector. O. Biebel made very helpful suggestions for data sources. Useful hints on locating nuclear data were supplied by F. Ajzenberg-Selove and H. Taub.

XVIII. APPENDIX

Cross Section Estimates

We have used partial cross sections and raw data found in the literature to make estimates of total inclusive cross sections for four massive particles. The fact that experimenters themselves did not present total cross sections testifies to the difficulty and large uncertainty associated with such calculations. Nevertheless the estimates made below may be useful within an order of magnitude.

J/ψ: Using a minimum bias trigger in a special run, CDF measured a cross section [23] for the prompt production of J/ψ with a value of

$$\sigma(p_t > 1.25, |y| < 0.6) = 2.86 \pm 0.01^{+0.34}_{-0.45}\, \mu b. \qquad (37)$$

Prompt J/ψ's are those which are consistent with originating at the beam line rather than from detached vertices. Since the entire p_t spectrum was measured for the J/ψ in this experiment, we used that information to correct the measured value upward by a factor of 1.28 before dividing by the effective interval $\Delta y = 1.2$. The result given below was divided by $(2J + 1) = 3$ and plotted in Fig. 5.

$$\frac{d\sigma(J/\psi)}{dy}\Big|_{y=0} = 3.06\ \mu\text{b}. \qquad (38)$$

D^{*+}: Using a detached vertex trigger, CDF measured the D^{*+} cross section as a function of p_t above $p_t = 6.0$ GeV/c [24]. We have used the J/ψ momentum spectrum as a guide to increase this cross section by a factor of 30.6 to account for the unmeasured portion of the p_t spectrum. Dividing by the effective rapidity interval of $\Delta y = 2$, we estimate

$$\frac{d\sigma(D^{*+})}{dy}\Big|_{y=0} = 0.075\ \text{mb}. \qquad (39)$$

This value is divided by $(2J + 1) = 3$ and plotted in Fig. 5.

Ξ_b^-: CDF has reported 17.5 of these events with a decay mode of $\Xi_b^- \to J/\psi\, \Xi^-$ [58].

We divide this number by integrated luminosity $L = 1.9\,\text{fb}^{-1}$ and multiply by 10 to correct for J/ψ acceptance over the rapidity range when J/ψ momentum is $p_t > 3.0$ GeV/c. We multiply by 3.26 to correct the unobserved J/ψ momentum spectrum below $p_t = 3.0$ GeV/c using the p_t spectra of reference [23] as a guide. We divide by 0.0593 to correct for the branching fraction of J/ψ into the observed $\mu^+\mu^-$ pair [18] and multiply by 10^3 to estimate a typical probability for hadron decay into J/ψ. Dividing the resulting cross section by $\Delta y = 2$, we obtain

$$\frac{d\sigma(\Xi_b^-)}{dy}\Big|_{y=0} = 2.53 \times 10^{-6}\ \text{mb}. \qquad (40)$$

We have divided this number by $(2J + 1) = 2$ and plotted it in Fig. 5.

B^+: CDF has measured the cross section at $\sqrt{s} = 1.96$ TeV for $p\bar{p} \to H_b X$, where X is anything and H_b includes b hadrons and anti b hadrons [23].

$$\sigma(p\bar{p} \to H_b X, |y| < 0.6) = 17.6 \pm 0.4^{+2.5}_{-2.3}\ \mu\text{b}. \qquad (41)$$

We divide this by 2 to obtain a cross section only for hadrons and by $\Delta y = 1.2$ to estimate $d\sigma/dy$. The B^+ cross section can be estimated using the branching fraction $B(b \to B^+) = 0.398 \pm 0.012$ [18] as a multiplier. The resulting cross section estimate for B^+ production is

$$\frac{d\sigma(B^+)}{dy}\Big|_{y=0} = 2.92\,\mu\text{b}. \qquad (42)$$

We have further reduced this value by 10% in an effort to scale it to a collision energy of $\sqrt{s} = 1.8$ TeV and divided by $(2J+1) = 1$ for plotting in Fig. 5.

[1] T. Alexopoulos, et al., Phys. Rev. Lett. **60** (1988) 1622.
[2] T. Alexopoulos, et al., Phys. Rev. Lett. **64** (1990) 991.
[3] T. Alexopoulos, et al., Phys. Rev. **D48** (1993) 984.
[4] T. Alexopoulos, et al., Phys. Lett. **B336** (1994) 599.
[5] T. Alexopoulos, et al., Phys. Rev. Lett. **71** (1998) 1490.
[6] T. Alexopoulos, et al., Z. Phys. **C67** (1995) 411.
[7] T. Alexopoulos, et al., Phys. Rev. **D62** (2000) 072004.
[8] T. Alexopoulos, et al., Phys. Rev. **D46** (1992) 2773.
[9] J. Gannon, et al., "Flying Wires at Fermilab", Proceedings of the 1989 IEEE Particle Accelerator Conference, (1989) 68.
[10] C.D. Moore, et al., "Single bunch intensity monitoring system using an improved wallcurrent monitor", Proceedings of the 1989 IEEE Particle Accelerator Conference, (1989) 1513.
[11] N. Gelfand, Fermilab Report FN-538, (1990).
[12] C. Grosso-Pilcher and S. White, Fermilab Report FN-550, (1990).
[13] K. Gulbrandsen, Senior Thesis, University of Wisconsin (1997).
[14] Private communication from S. Oh.
[15] R.D. Field and R.P. Feynman, Nucl. Phys. **B136** (1978) 1.
[16] See for example discussions and references in G. Bocquet, et al., Phys. Lett. **B366** (1996) 447.
[17] V.V.Anisovich and V.M. Shekhter, Nucl. Phys. **B55** (1973) 455, V.V. Anisovich and V.M. Shekhter, Phys. Lett.**B52** (1974) 217. These authors also attempt to make higher order corrections to inclusive cross sections to account for contributions from decays of higher mass particles and resonances without making any allowance for mass dependence of cross sections.
[18] C. Amsler, et al., (Particle Data Group), Physics Letters **B667**, (2008) 1.
[19] R. Hagedorn and J. Rafelski, Phys. Lett. **B97** (1980) 136.
[20] P. Levai and B. Müller, Phys. Rev. Lett. **67** (1991) 1519.
[21] T. Alexopoulos, et al., Phys. Rev. **D48** (1993) 1931.
[22] R. Hagedorn, Nuovo Cimento Supplemento **6** (1968) 311.
[23] D. Acosta, et al., CDF Collaboration, Phys. Rev. **D71**, (2005) 032001 .
[24] D. Acosta, et al., CDF II Collaboration, Phys. Rev. Lett. **91** (2003) 241804.
[25] A. Abulencia, et al. CDF Collaboration, Phys. Rev. **D75**, (2007) 012010 .
[26] J.W. Cronin, et al., Phys. Rev. **D11** (1975) 3105.
[27] See for example V.D. Barger and R.J.N. Phillips, Collider Physics, (1987) Addison-Wesley Publishing Company. Applications can be found in R.D. Field and R.P. Feynman, Nucl. Phys. **B136** (1978) 1.
[28] Although the observed momentum spectrum for B^+ production is not exponential, it does not scale as the lower mass particles do in the momentum range studied.
[29] C. Amsler, et al., (Particle Data Group), Physics Letters **B667** (2008) 355. The table for e^+e^- multiplicities was updated Aug. 2007 by O. Biebel.
[30] Ibid., 946.
[31] Ibid., 399.
[32] G. Alexander, et al., Physics Letters **B384** (1996) 343.
[33] M. Cacciari and P. Nason, JHEP **09**, (2003) 06.
[34] D. Kharzeev, K. Tuchin, Nucl. Phys. **A753** (2005) 316.
[35] J.S. Schwinger, Phys. Rev. **82** (1951) 664.
[36] S.W. Hawking, Commun. Math. Phys. **43** (1975) 199 and W.G.Unruh, Phys. Rev. **D14** (1976) 870.
[37] P. Castorina, D. Kharzeev, H. Satz, Eur.Phys. J. **C52** (2007) 187, arXiv: 0704.1426v2 [hep-ph] (2007).
[38] F. Becattini, P. Castorina, J. Manninen, H. Satz, Eur. Phys. J. **C56** (2008) 493, arXiv: 0805.0964v1 [hep-ph] (2008).
[39] Steven Frautschi, Phys. Rev. **D3** (1971) 2821.
[40] R. Hagedorn, Nucl. Phys. **B24** (1970) 93.
[41] S.R. deGroot, W.A. van Leeuwen, Ch.G. vanWeert, Relativistic Kinetic Theory, (1980) North-Holland Publishing Company.
[42] See for example F. Reif, Fundamentals of Statistical and Thermal Physics, McGraw-Hill (1963) 313.
[43] F. Jüttner, Ann. Physik u. Chemie **34** (1911) 856.
[44] F. Jüttner, Z. Phys. **47** (1928) 542.
[45] T. Affolder, et al., CDF Collaboration, Phys. Rev. Lett. **87** (2001) 141802.
[46] F. Abe, et al., CDF Collaboration, Phys. Rev. **D50** (1994) 5535.
[47] S. Klimenko, J. Konigsberg, and T.M. Liss, Fermilab Technical Note FN-0741.
[48] $\sqrt{s} = 63$ GeV: T. Åkesson, et al., Axial Field Spectrometer Collaboration, Nucl. Phys. **B203** (1982) 27.
$\sqrt{s} = 200$ GeV: J. Adams, et al., STAR Collaboration, Phys. Lett. **B612** (2005) 181, and J. Dunlop, private communication.
[49] M. Froissart, Phys. Rev. **123** (1961) 1053.
[50] W.R. Webber, et al., Phys. Rev. **C41** (1990) 547.
[51] N. Crayton, et al.,Rev. Mod. Phys. **14** (1962) 186.
[52] H. Hotchi, et al., Phys. Rev. **C64** (2001) 044302.
[53] P. Salvisberg, et al., Phys. Rev. **C46** (1992) 2172.
[54] B.L. Berman, et al.,Phys. Rev. **C51** (1995) 1882.
[55] T. Alexopoulos, et al., Phys. Lett. **B528** (2002) 43.
[56] This relation has the same inverse dependence of temperature on size as that obtained by S. Weinberg for expanding black body radiation. "The First Three Minutes", A Mathematical Supplement, (1977) Bantum Books.
[57] Gary Steigman, Annu. Rev. Nucl. Part. Sci., **57** (2007)

463.
[58] T. Aaltonen et al. CDF Collaboration, Phys. Rev. Lett. **99** (2007) 052002 . A similar number of events was reported also by V.M. Abazov et al. D0 Collaboration, Phys. Rev. Lett. **99** (2007) 052001 .